対流混合層の
シミュレーションと解析

伊藤　純至

解像度に応じたシミュレーションの区別

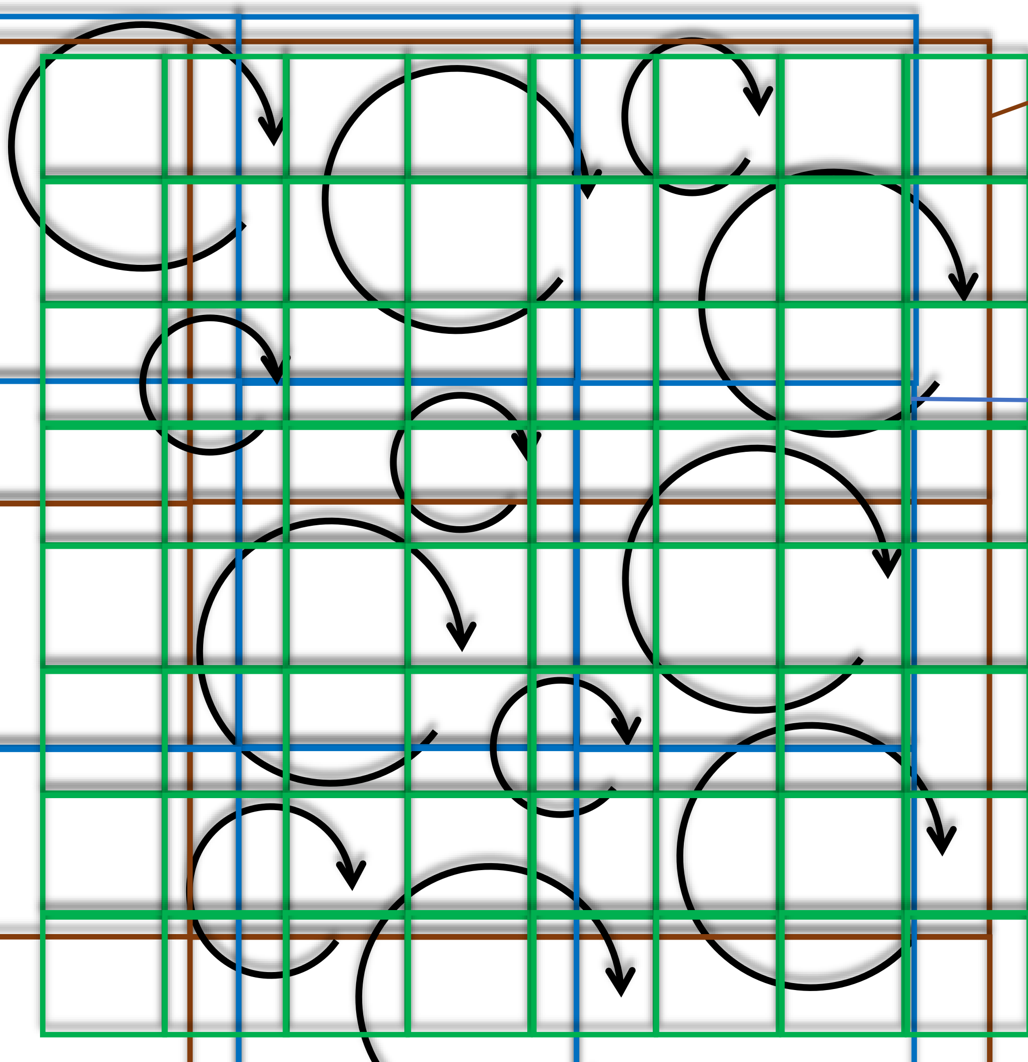

*解像度*とサブグリッドモデルで表現するべきもの

***従来の気象モデルの粗い解像度*：多数の乱流渦の寄与の統計平均**
- 乱流輸送は大・ゆらぎは小
- 統計的に一様とみなせる場合、乱流輸送なし

***中程度の解像度*：単一の大きな渦の寄与**
- 乱流輸送は大・ゆらぎは大

***LESのような高い解像度*：小さな渦の寄与**
- 乱流輸送は小・ゆらぎは大

グレーゾーン：パラメタリゼーション設計が最も困難

RANS・グレーゾーン・LES

- RANS: 対流混合層の輸送過程全体をパラメタライズ：高次モデルやNon-localモデルが気象モデルで利用されているが、不確定性は大きい

- グレーゾーン：何らかのパラメタライズは必須だが未解決

- LES：それなりに信頼できる。計算量やデータ量が膨大になりがち

LESの定義

- 教科書的

→ 乱流の慣性小領域以下のサイズに格子間隔を設定し、・・・

現実的な対象について、満足することは難しい。強い安定成層時は不可能

- 広義

→ 小スケールの主要な変動が、格子状で陽に再現された数値計算

微妙な場合はLarge Eddy Permitting-Modelと呼んでいる場合も

最初のLES

J. Fluid Mech. (1970), *vol.* 41, *part* 2, *pp.* 453–480 453
Boeing Symposium on Turbulence

A numerical study of three-dimensional turbulent channel flow at large Reynolds numbers

By JAMES W. DEARDORFF
National Center for Atmospheric Research, Boulder, Colorado 80302

(Received 9 May 1969)

The three-dimensional, primitive equations of motion have been integrated numerically in time for the case of turbulent, plane Poiseuille flow at very large Reynolds numbers. A total of 6720 uniform grid intervals were used, with sub-grid scale effects simulated with eddy coefficients proportional to the local velocity deformation. The agreement of calculated statistics against those measured by Laufer ranges from good to marginal. The eddy shapes are examined, and only the u-component, longitudinal eddies are found to be elongated in the downstream direction. However, the lateral v eddies have distinct downstream tilts. The turbulence energy balance is examined, including the separate effects of vertical diffusion of pressure and local kinetic energy.

It is concluded that the numerical approach to the problem of turbulence at large Reynolds numbers is already profitable, with increased accuracy to be expected with modest increase of numerical resolution.

- Deardorff (1970)が発端
- その後、工学分野（例えば機械・航空・建築等）で普及

Deardroff (1974)のLES

- 対流混合層
- 領域:水平5km×5km×鉛直2km
- 格子数:40×40×40

- 対流混合層の
グリッド上で解像

観測と整合する
鉛直プロファイル

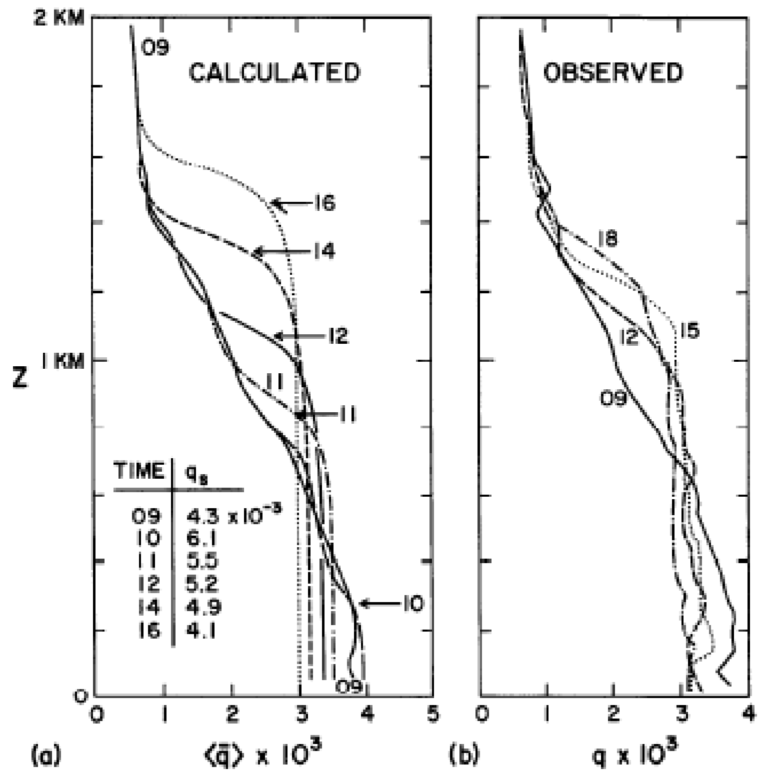

Fig. 2a. Numerically calculated profiles of specific humidity during DAY 33. Calculated values for the ground surface, q_s, are listed in lower left portion.
Fig. 2b. Observed profiles of specific humidity during DAY 33 from Clarke *et al.* (1971).

スーパーコンピューター性能の向上

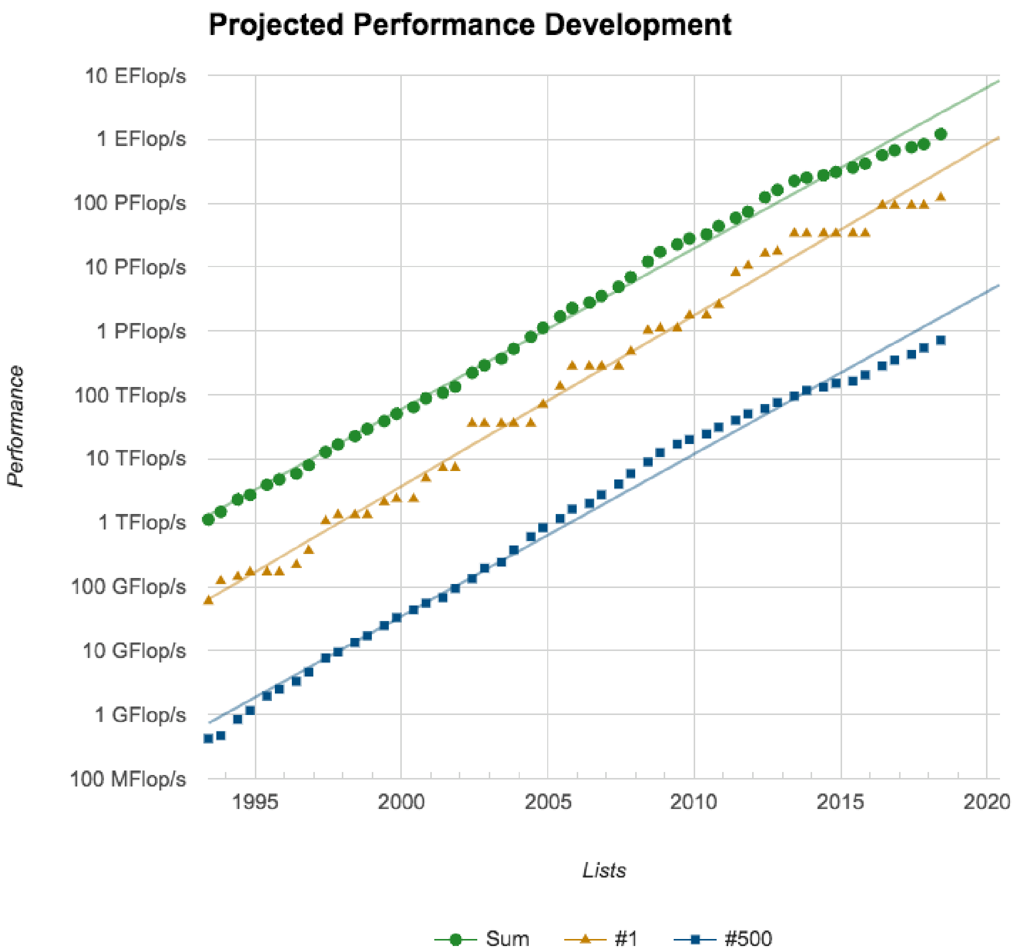

→大規模なLESが可能

台風のLES：
格子数20000X20000X60

Top500　webサイトより

対流混合層のLES比較実験

P4.7 ENTRAINMENT INTO SHEARED CONVECTIVE BOUNDARY LAYERS AS PREDICTED BY DIFFERENT LARGE EDDY SIMULATION CODES

Evgeni Fedorovich* and Robert Conzemius
School of Meteorology, University of Oklahoma, Norman, Oklahoma

Igor Esau
Nansen Environmental and Remote Sensing Center, Bergen, Norway

Fotini Katopodes Chow
Environmental Fluid Mechanics Laboratory, Stanford University, California

David Lewellen
Department of Mechanical and Aerospace Engineering, West Virginia University, Morgantown, West Virginia

Chin-Hoh Moeng and Peter Sullivan
National Center for Atmospheric Research, Boulder, Colorado

David Pino
Institute for Space Studies of Catalonia and Department of Applied Physics, Technical University of Catalonia, Barcelona, Spain

Jordi Vilà-Guerau de Arellano
Department of Meteorology and Air Quality, Wageningen University, Netherlands

AMS boundary layer conference(2014)のextended abstract

実験設定：成層と地衡流

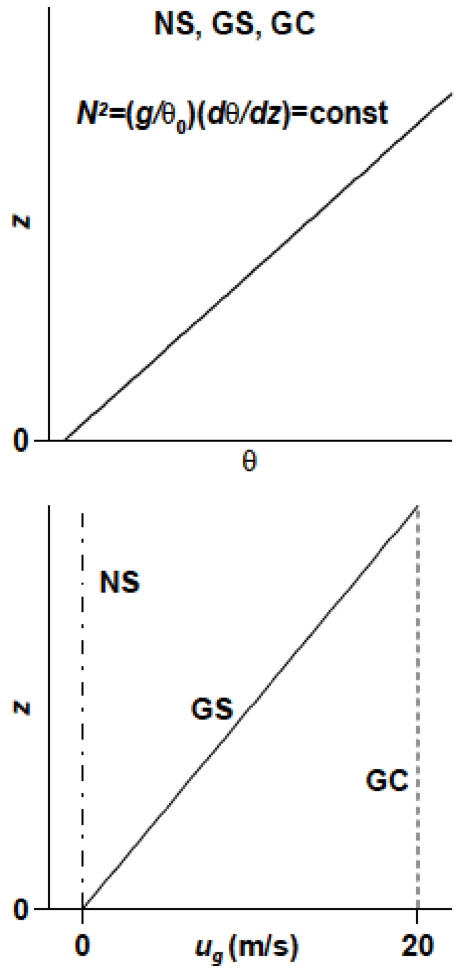

Figure 1. Initial profiles of the virtual potential temperature θ and x component of the geostrophic wind velocity, u_g, for the simulated CBL cases.

初期成層一様

6つの異なるLESモデル（解像度も同一でない）の計算結果を比較

NS: 無風
GS: 地衡風線形増加
GC: 地衡風一様

左：温位と右：θ^2の鉛直分布の比較

NS

GC

GS

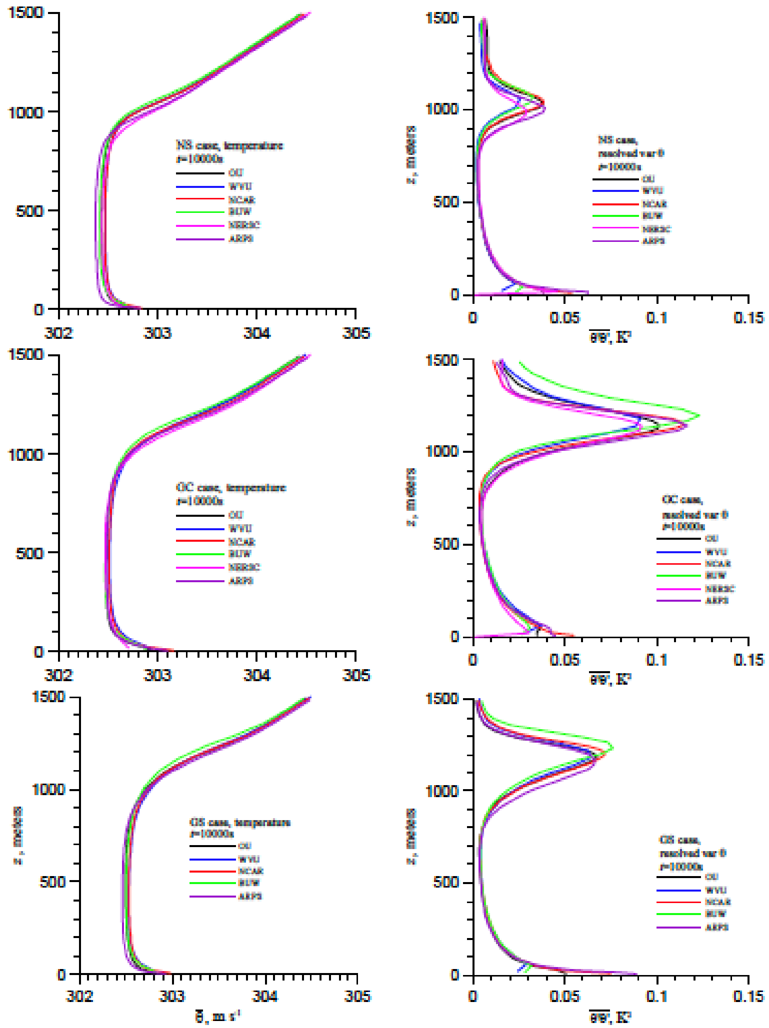

Figure 2. Profiles of the mean virtual potential temperature (right-hand plots) and resolved temperature variance (left-hand plots) for all three simulated cases (NS, GC, and GS, see section 2) at t=10000s.

鉛直熱フラックス（左：合計と右：サブグリッド成分）

NS

GC

GS

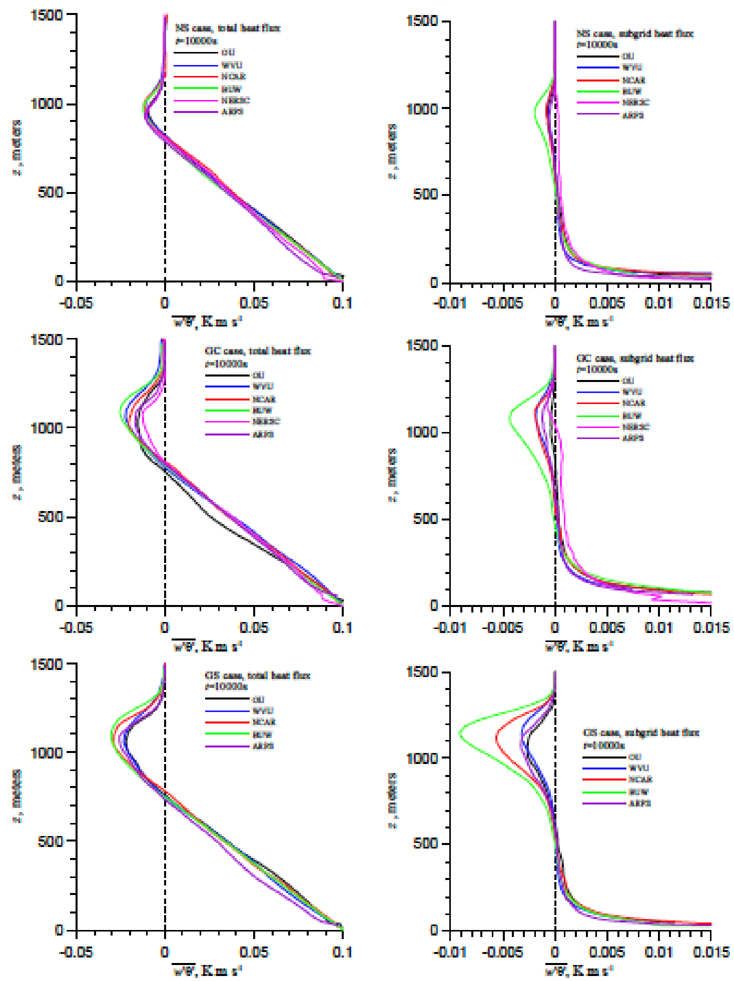

Figure 3. Vertical kinematic heat flux (left-hand plots: total=resolved+subgrid; right-hand plots: subgrid) for all three simulated cases (NS, GC, and GS, see section 2) at t=10000s.

左：u'^2と右：w'^2の鉛直分布

NS

GC

GS

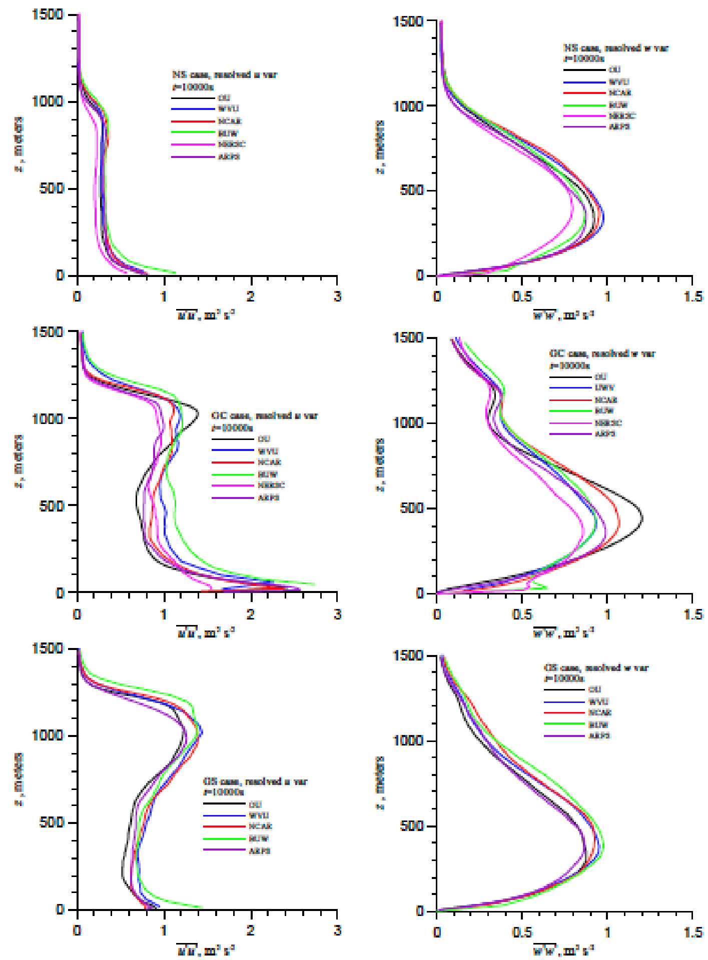

Figure 4. Variances of the resolved *u* (left-hand plots) and *w* (right-hand plots) velocity components for all three simulated cases (NS, GC, and GS, see section 2) at *t*=10000s.

左：w'^3と右：$\theta'^2 w'$の鉛直分布

NS

GC

GS

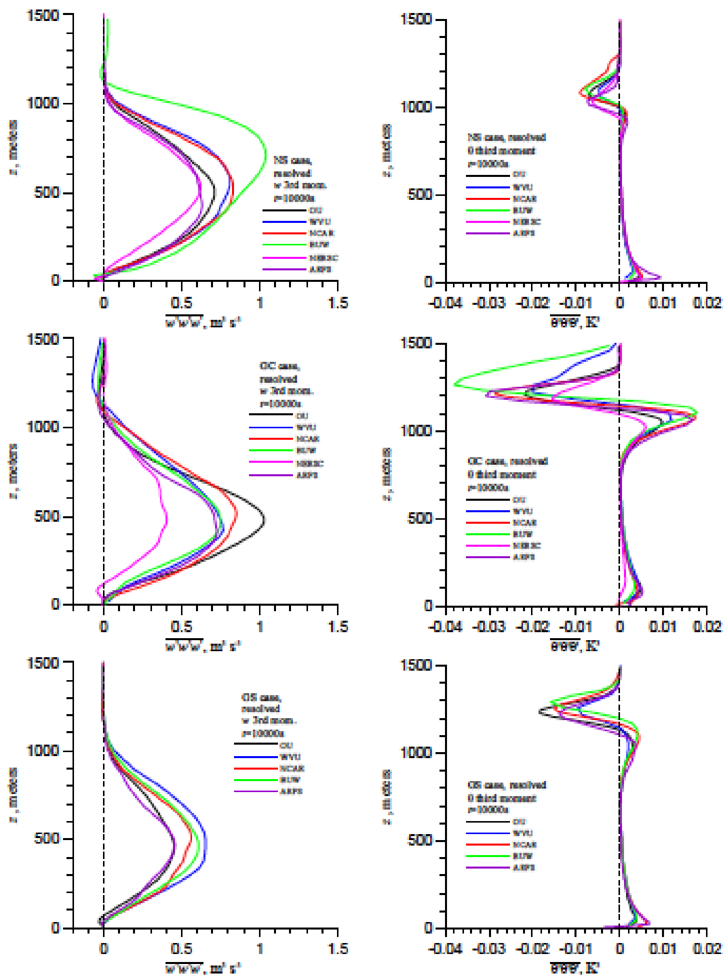

Figure 5. Third moments of the resolved vertical velocity (left-hand plots) and virtual potential temperature (right-hand plots) for all three simulated cases (NS, GC, and GS, see section 2) at t=10000s.

UとVの分布

GC

GS

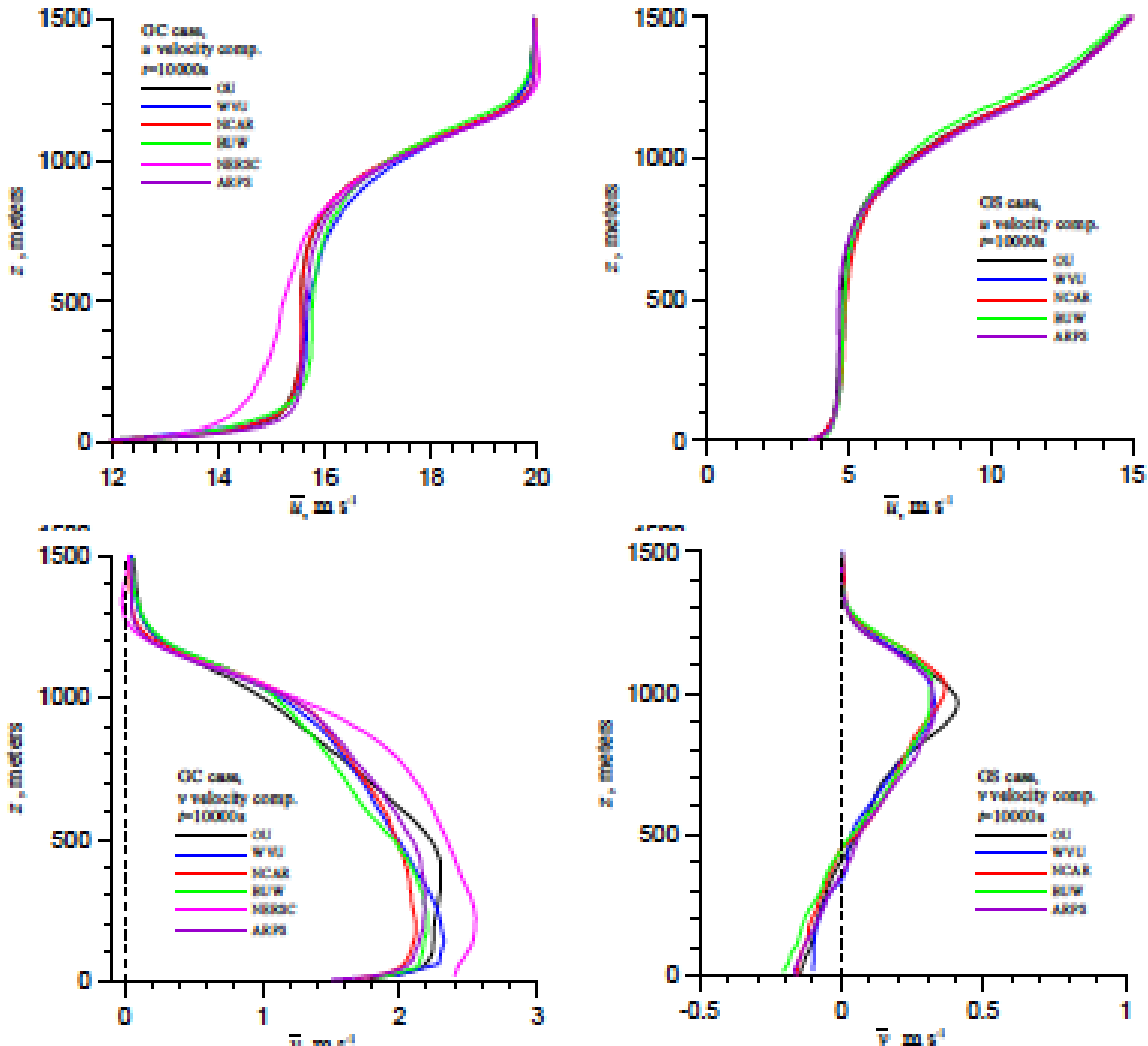

1500
1000
500
0
z, meters
12
14
16
18
20
0
5
10
15
-0.5
0.5
1
2
3
OU
WVU
NCAR
NERSC
ARPS

LES_AORI_NDAの開発

～NCARのMoeng(NCAR)さん、近藤さん(産総研)らのモデル

Nakanishi(2000)の放射霧のLES、雲粒（液水温位）と放射過程

↓

ベクトル機（地球シミュレータ）向けコード、中西さんがHPで配布

ブシネスク近似　→　成層流体にも関わらず非圧縮性流体の取り扱いが可能

<長所>

- Δtを大きく設定できる

<欠点>

- 密度変化が大きい場合は不適切（積雲対流・火星の対流混合層）
- ポアソン方程式→全体通信が必要

→

田中ら（気象研究ノート）の塵旋風のLES

↓

伊藤が使用(2007～)、派生バージョンいろいろ（ダスト、雲(Nakamura 1976)、SGSモデル、移流スキーム等）、基本的にはドライ専用、Fortran90

↓

（現在）「京」やその他大型計算機に向けてスカラー並列化が完了・湿潤過程を再導入

LES_NDA_AORIの並列化

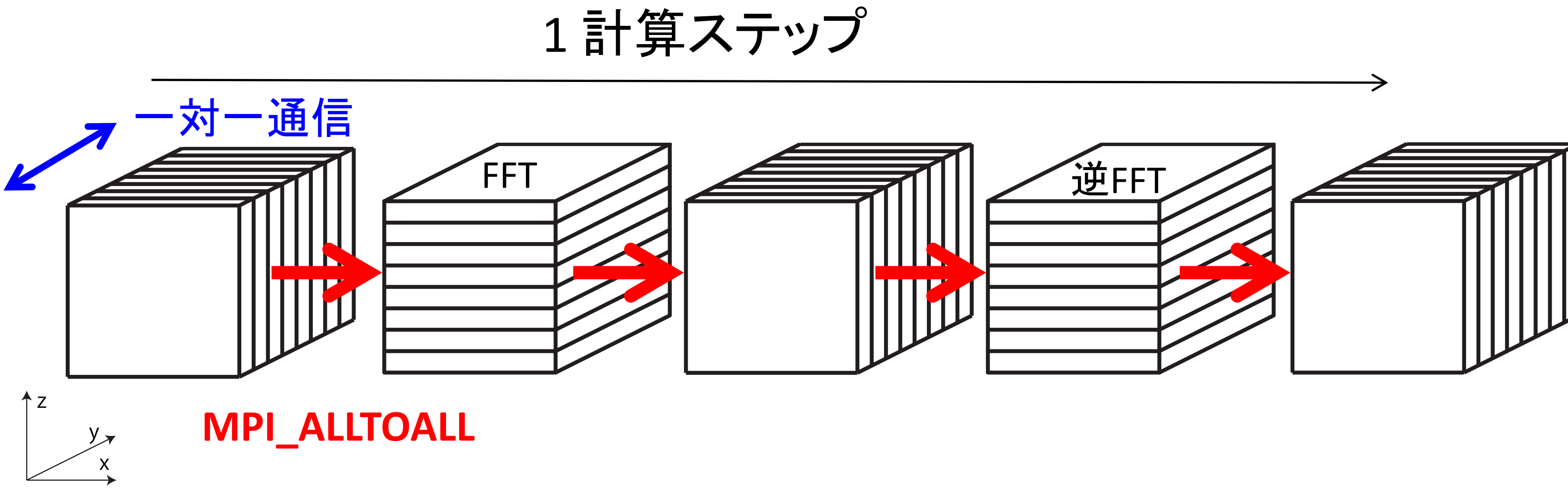

y-方向分割
移流・SGSなど+IO
z方向スレッド並列

z-方向分割
xy-方向ポアソン方程式
xy-方向2次元FFT

y-方向分割
z-方向ポアソン方程式
三重対角行列

z-方向分割
xy-方向ポアソン方程式
xy-方向2次元逆FFT

ポアソン方程式では緩和法を利用しない
→　非圧縮性流体方程式ながら、高並列化効率が期待

Strong Scaling

格子数360*360*240（ダストデビル実験のΔ=12.5mに相当）でのベンチマーク

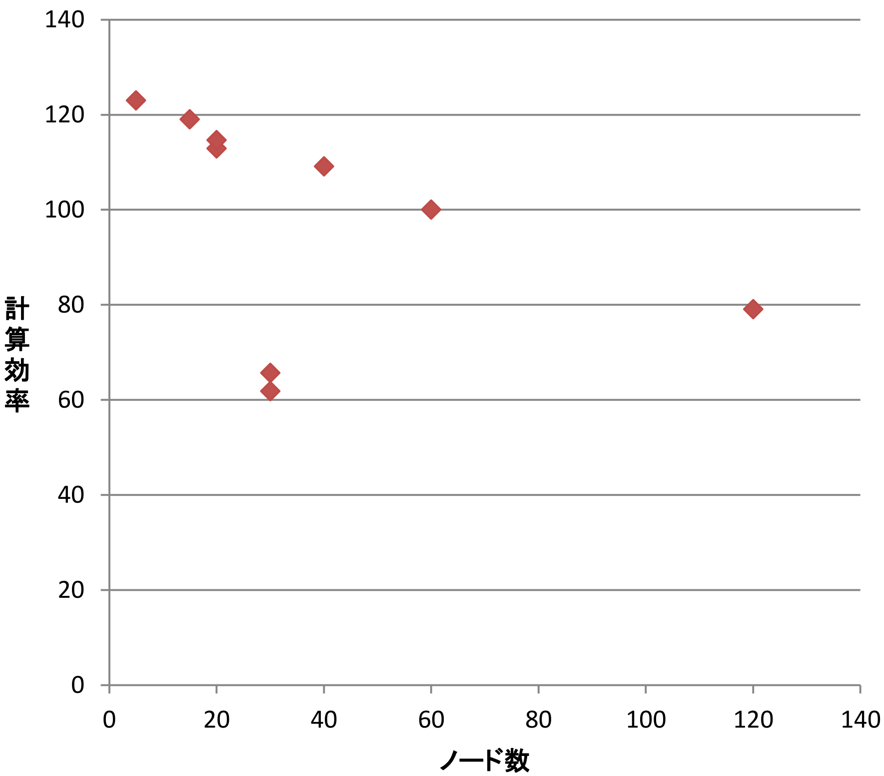

まあまあの並列化効率
720*720*480も120ノードから240ノードで75%以上は達成

並列数は水平格子数と鉛直格子数の公約数でなければならない

FFTの計算コストはO(nlogn^2) → Weak scalingは単純でない

京コンピュータでの計算例：dx=2mの対流混合層のLES

解像度2mのLESで再現した対流混合層（ただし本研究のLESの解像度は25m)

地表面付近の水平断面のw

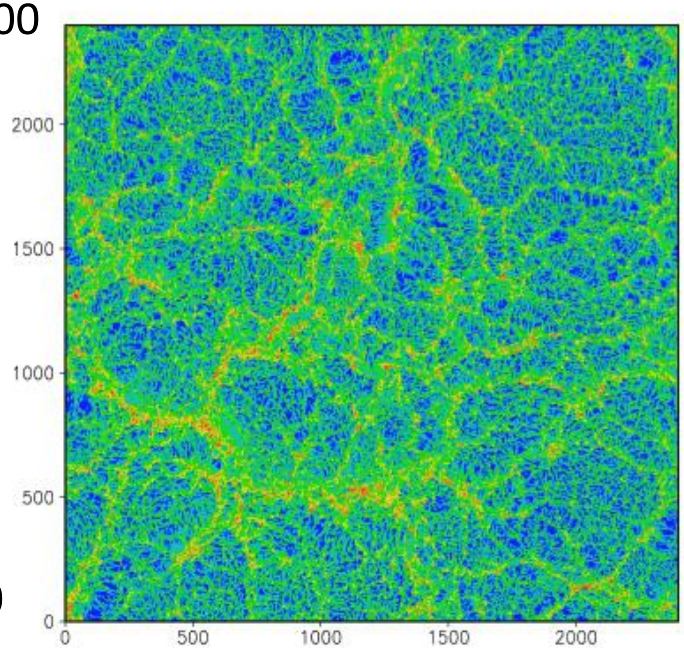

鉛直断面の温位θ

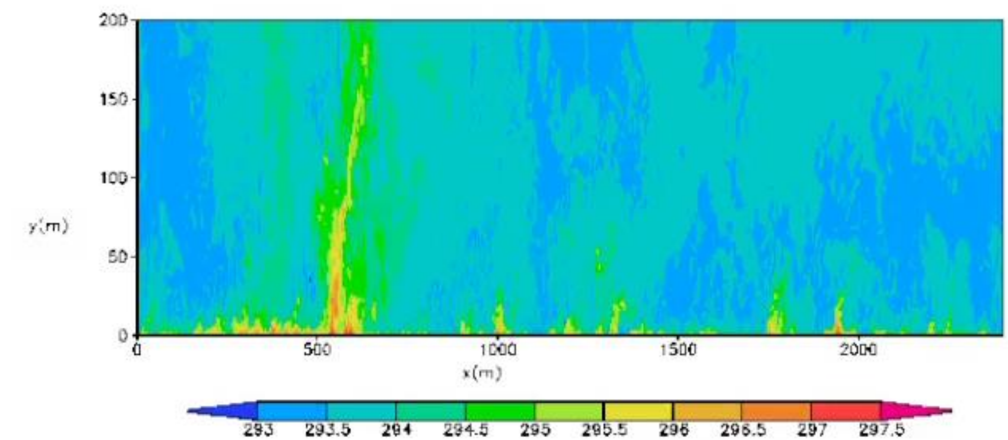

LES-NDA-AORIの検証：θ

NS

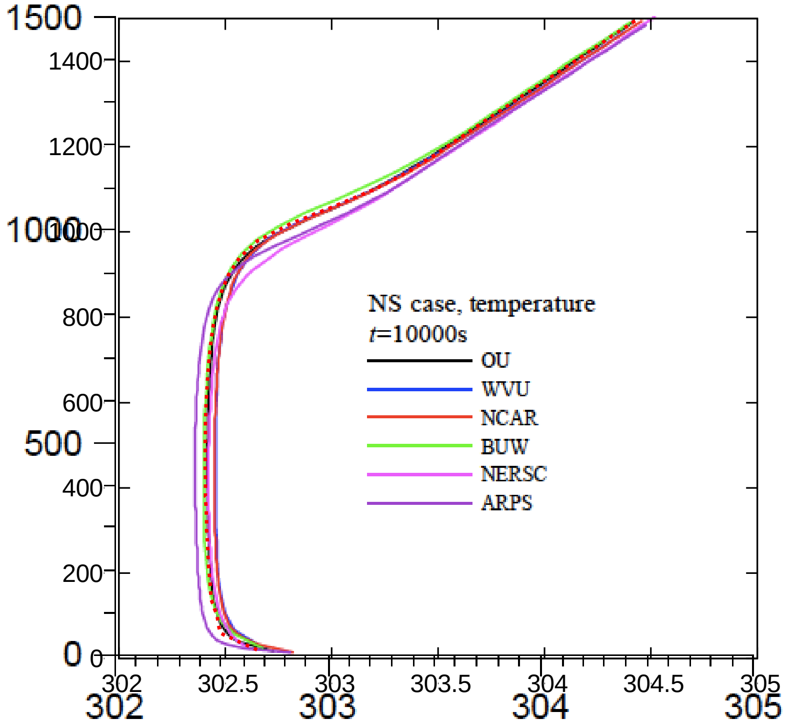

GC

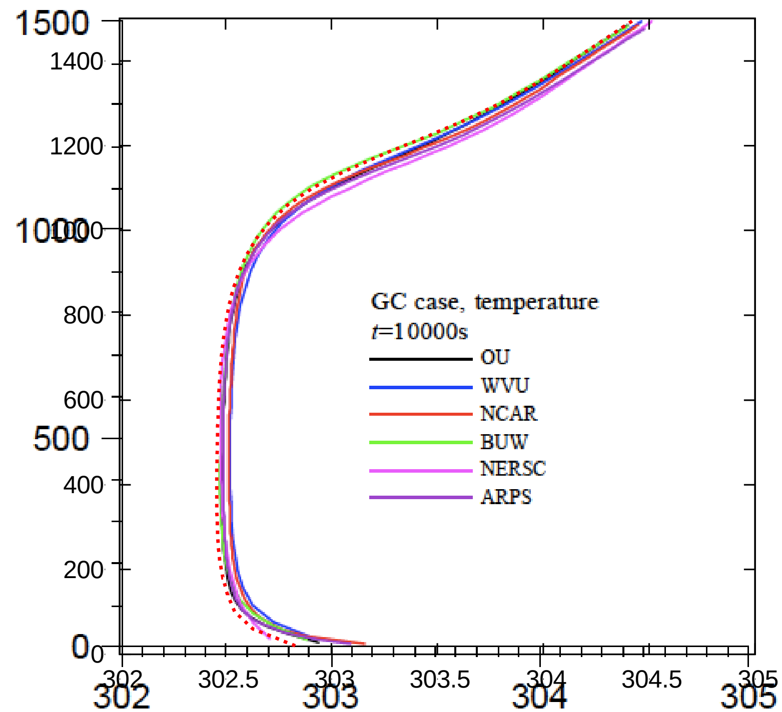

Θ'^2

NS

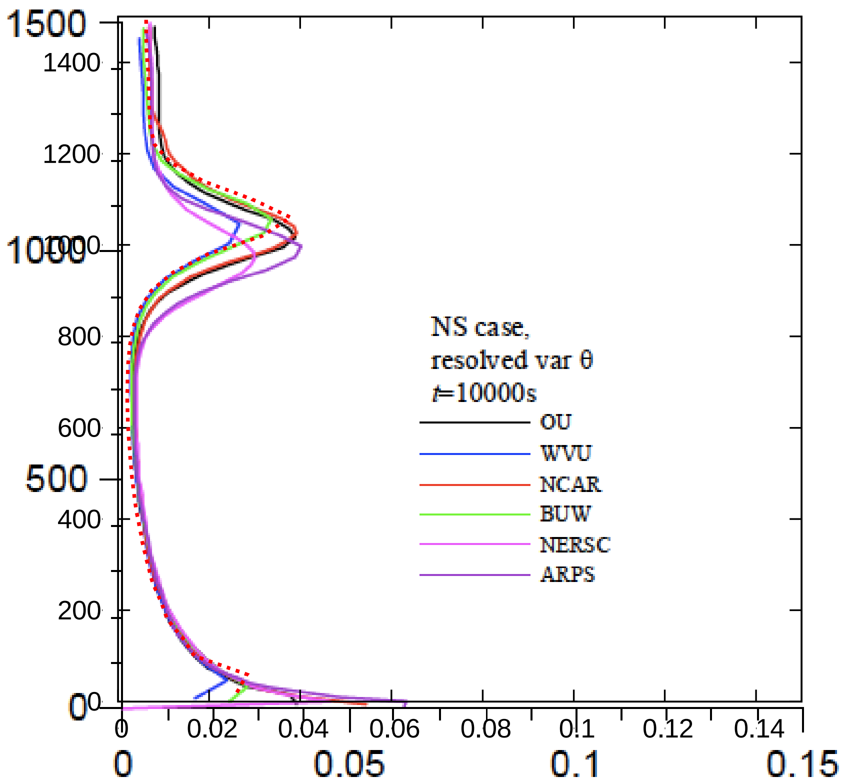
NS case,
resolved var θ
t=10000s
OU
WVU
NCAR
BUW
NERSC
ARPS
1500
1400
1200
1000
800
600
500
400
200
0
0.02
0.04
0.06
0.08
0.1
0.12
0.14
0.05
0.15

GC

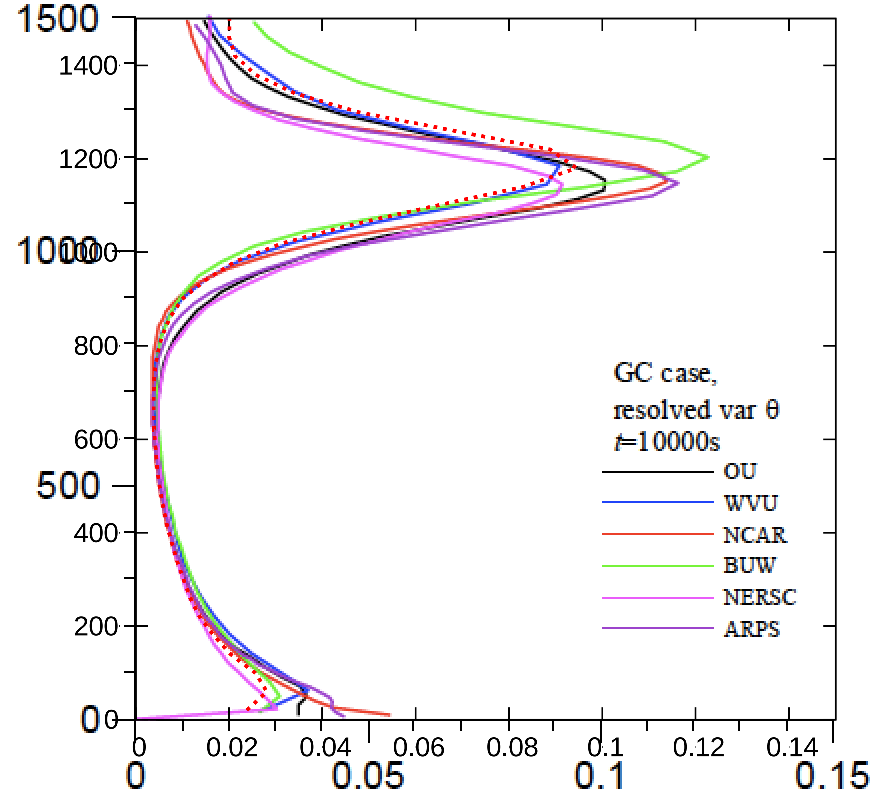
GC case,
resolved var θ
t=10000s
OU
WVU
NCAR
BUW
NERSC
ARPS
1500
1400
1200
1000
800
600
500
400
200
0
0.02
0.04
0.06
0.08
0.1
0.12
0.14
0.05
0.15

u'^2

NS

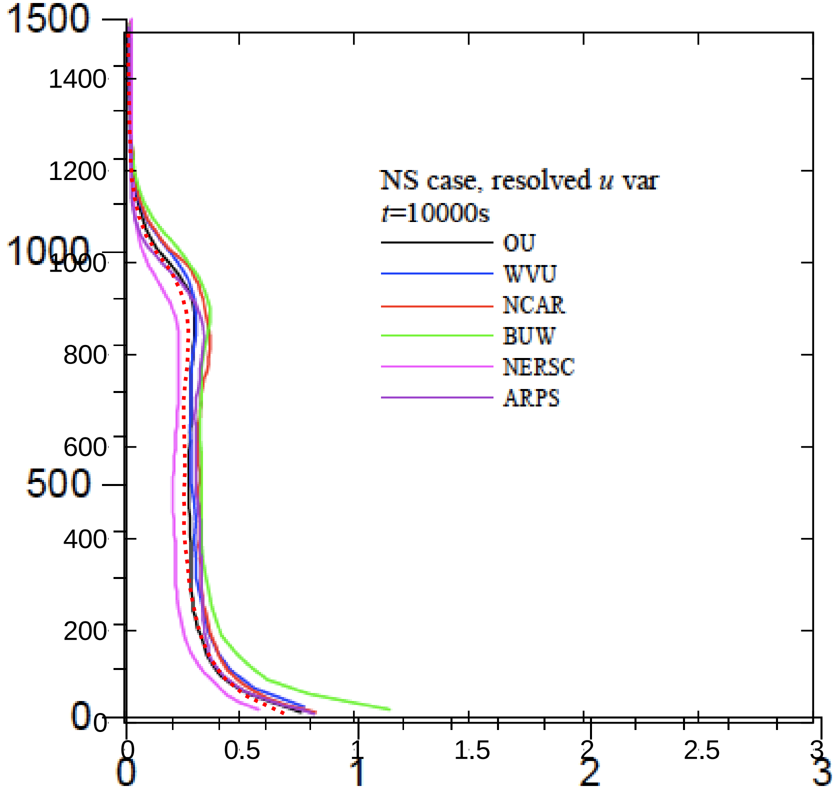
NS case, resolved *u* var
t=10000s
OU
WVU
NCAR
BUW
NERSC
ARPS
1500
1400
1200
1000
800
600
500
400
200
0
0.5
1
1.5
2
2.5
3

GC

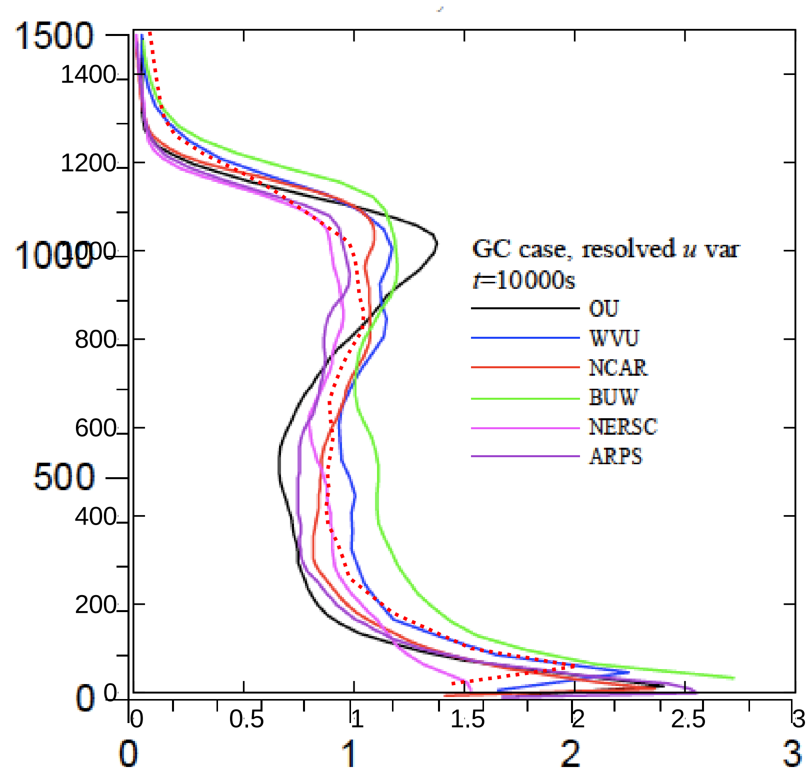
GC case, resolved *u* var
t=10000s
OU
WVU
NCAR
BUW
NERSC
ARPS
1500
1400
1200
1000
800
600
500
400
200
0
0.5
1
1.5
2
2.5
3

w'²

NS

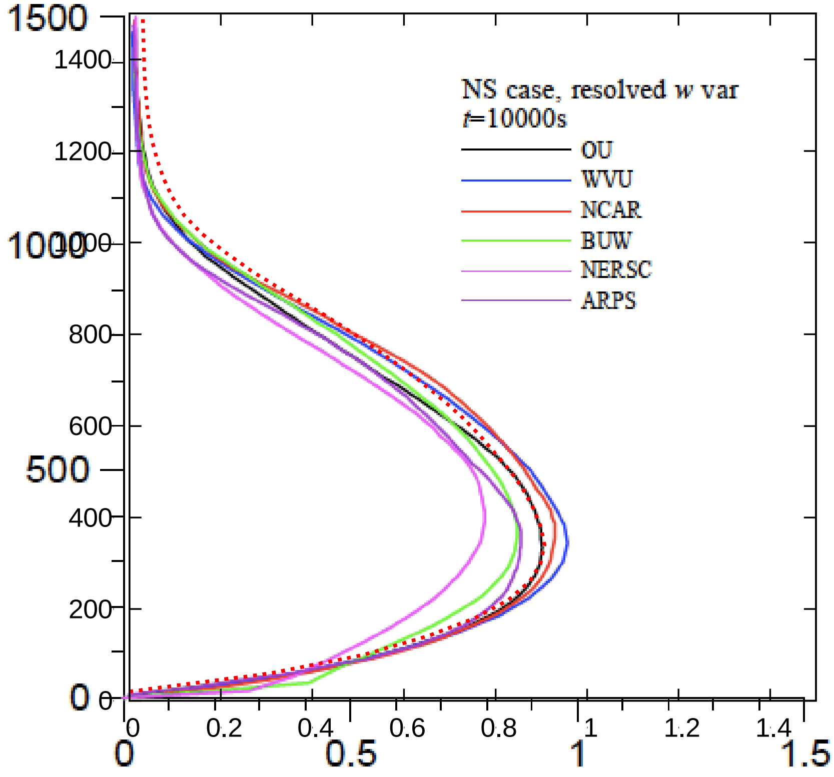

NS case, resolved *w* var
t=10000s
OU
WVU
NCAR
BUW
NERSC
ARPS
1500
1400
1200
1000
800
600
500
400
200
0
0.2
0.4
0.5
0.6
0.8
1
1.2
1.4
1.5

GC

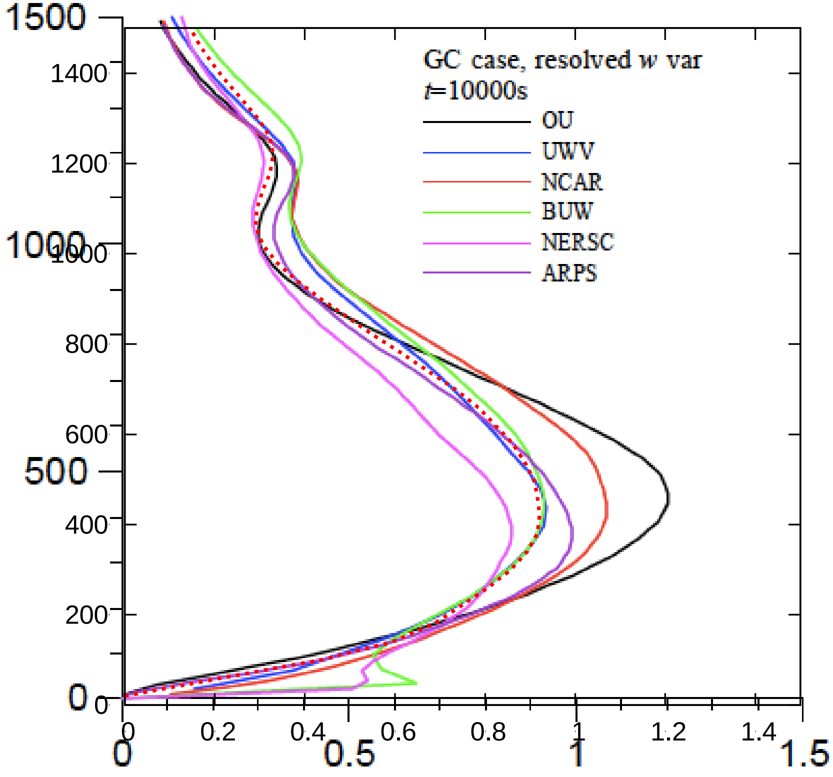

GC case, resolved *w* var
t=10000s
OU
UWV
NCAR
BUW
NERSC
ARPS
1500
1400
1200
1000
800
600
500
400
200
0
0.2
0.4
0.5
0.6
0.8
1
1.2
1.4
1.5

w'^3

NS

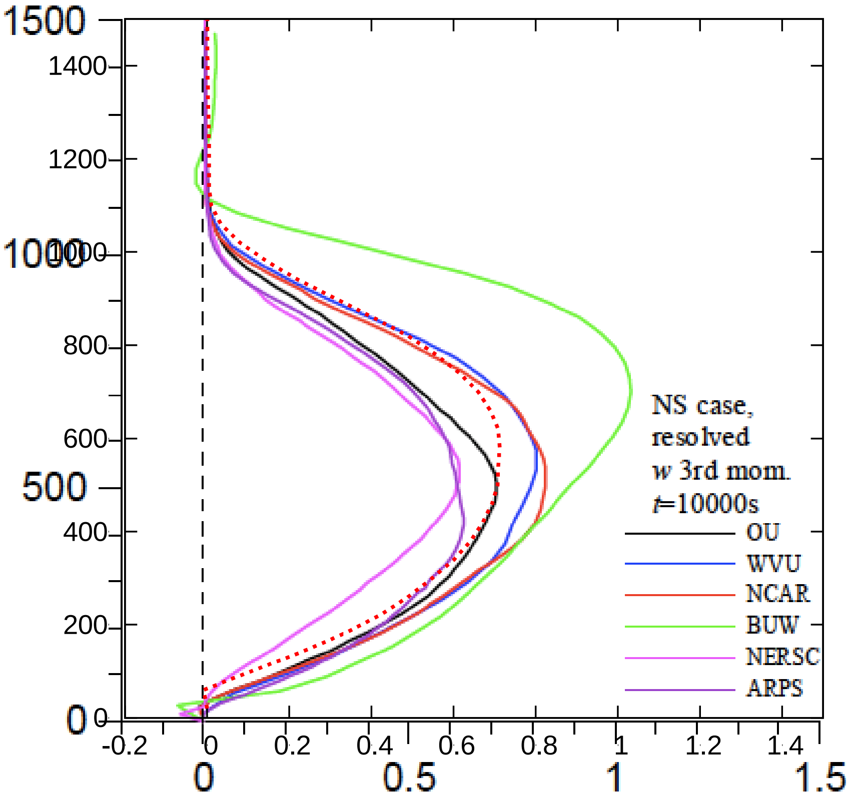
NS case,
resolved
w 3rd mom.
t=10000s
OU
WVU
NCAR
BUW
NERSC
ARPS
1500
1400
1200
1000
800
600
500
400
200
0
-0.2
0
0.2
0.4
0.6
0.8
1
1.2
1.4
0.5
1.5

GC

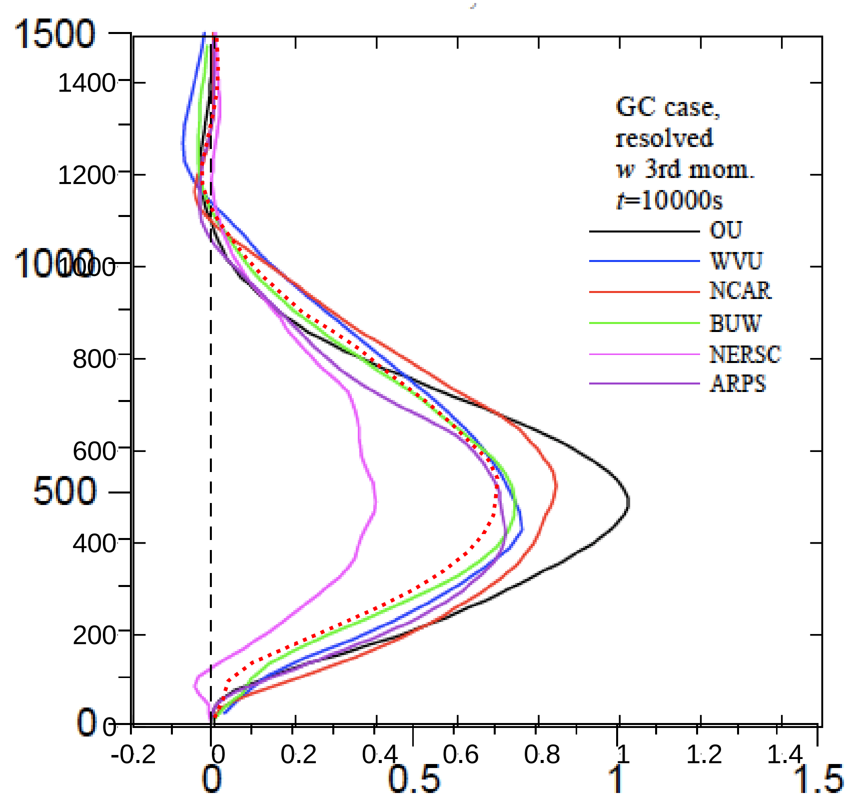
GC case,
resolved
w 3rd mom.
t=10000s
OU
WVU
NCAR
BUW
NERSC
ARPS
1500
1400
1200
1000
800
600
500
400
200
0
-0.2
0
0.2
0.4
0.6
0.8
1
1.2
1.4
0.5
1.5

θ^3

NS

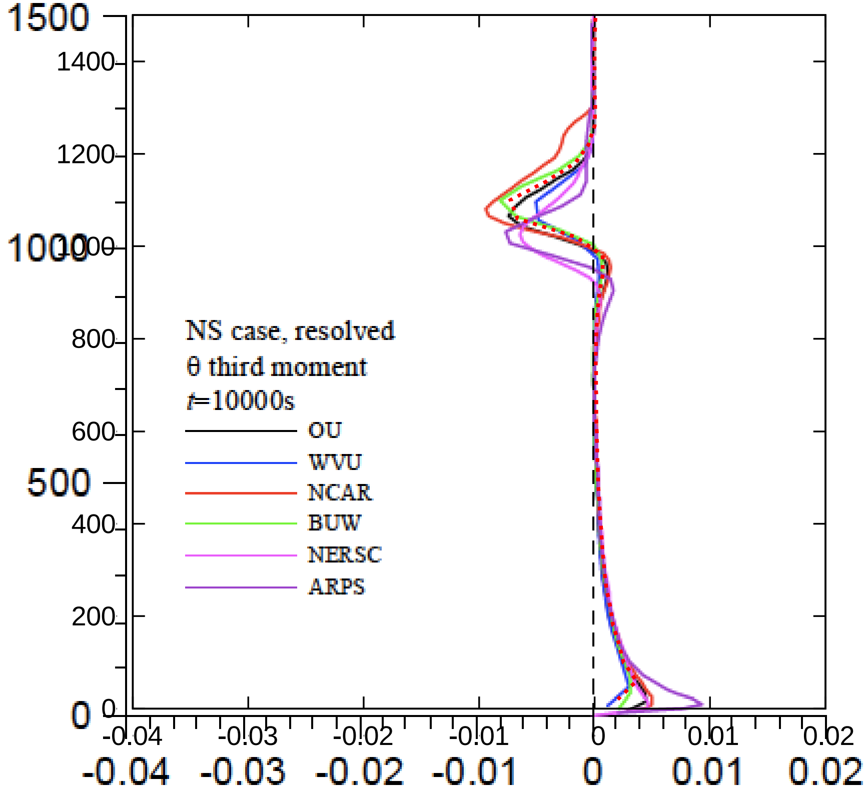

NS case, resolved
θ third moment
t=10000s
OU
WVU
NCAR
BUW
NERSC
ARPS
1500
1400
1200
1000
800
600
500
400
200
0
-0.04
-0.03
-0.02
-0.01
0
0.01
0.02

GC

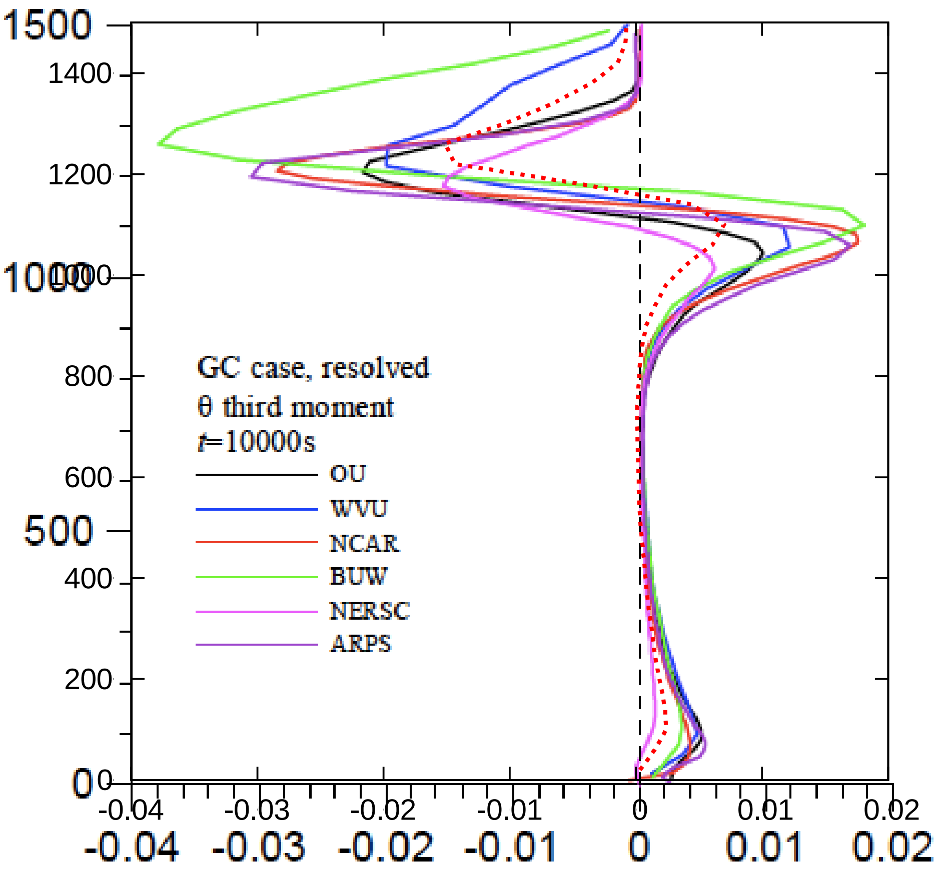

GC case, resolved
θ third moment
t=10000s
OU
WVU
NCAR
BUW
NERSC
ARPS
1500
1400
1200
1000
800
600
500
400
200
0
-0.04
-0.03
-0.02
-0.01
0
0.01
0.02

U and V in GC case

U

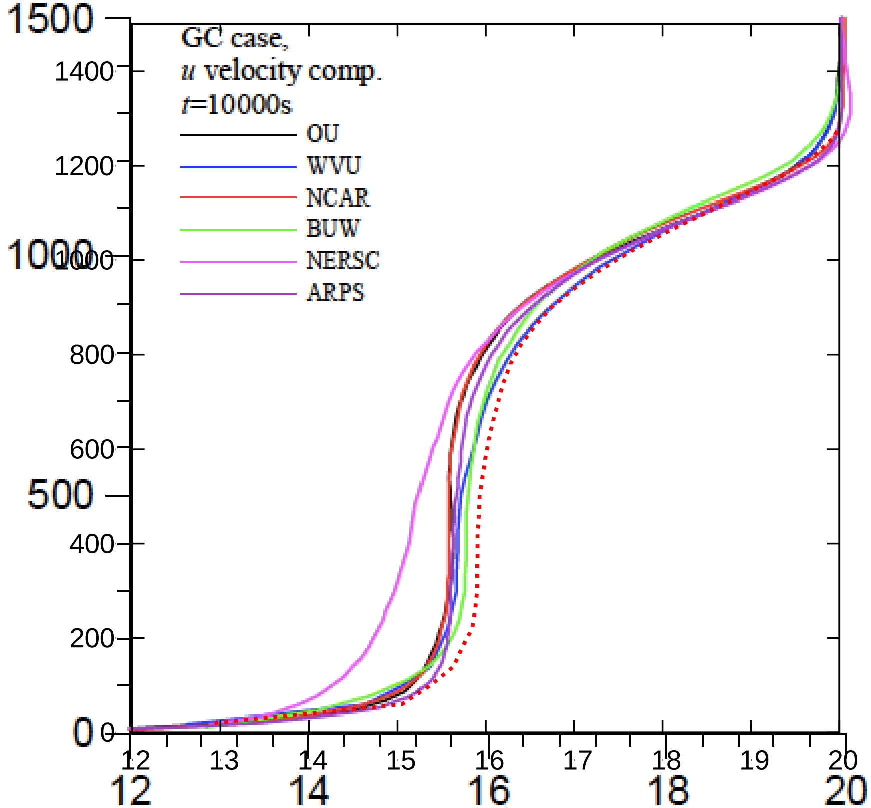

V

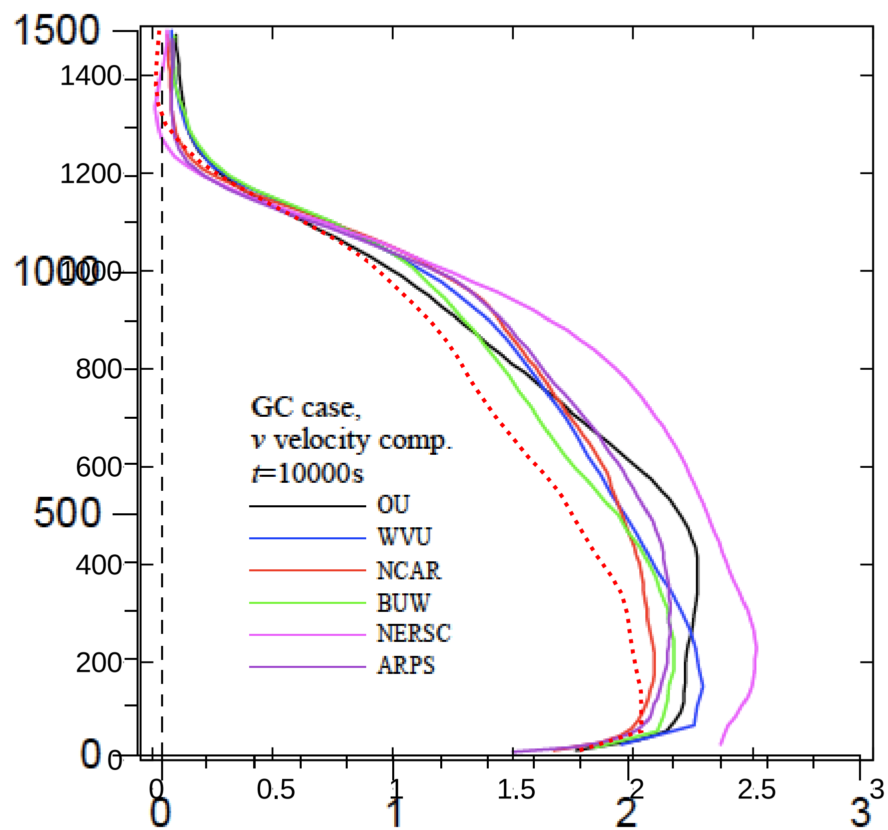

地表面フラックスの定式化の違いが影響？

湿潤LES

LES_AORI_NADの湿潤版
Liqud-water path

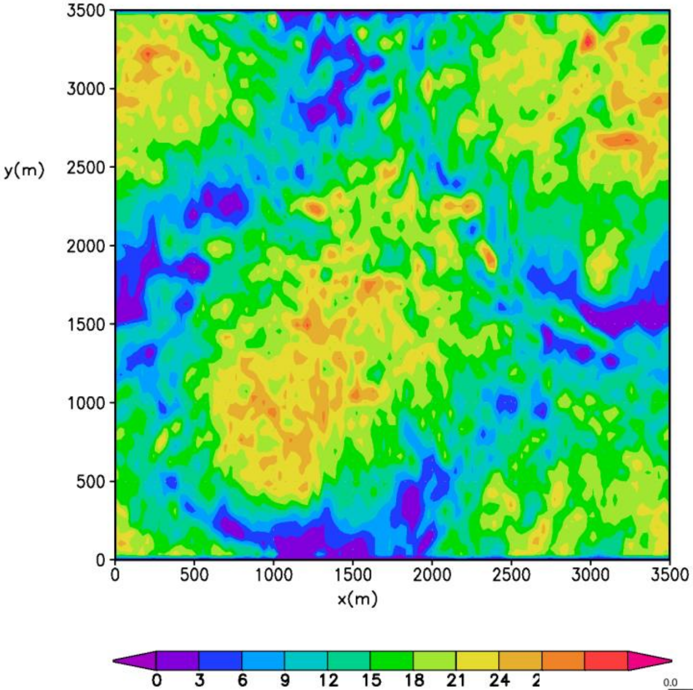

湿潤LESのモデル間比較
（Dycoms-2の層積雲、Stevens et al. (2003)）

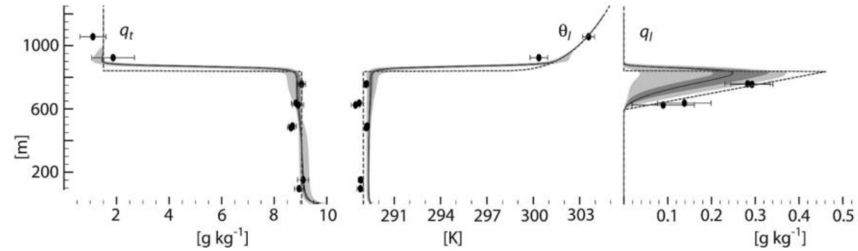

FIG. 4. Profile of mean state of specific humidity and temperature at initial time (dashed lines), as observed (points), and from master ensemble averaged over the fourth hour (solid lines). The shading is as in Fig. 2 and as described in the text.

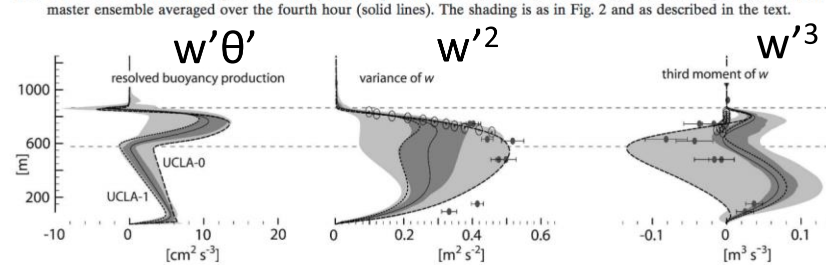

FIG. 5. Profile of vertical velocity statistics—(left) resolved buoyancy production, (middle) variance of *w*, and (right) third moment of *w*—from master ensemble averaged over the fourth hour. Markers indicate estimates of vertical velocity second and third moments as derived from in situ (solid with bar) and radar (circle–dot). Details of data analysis provided by Stevens et al. (2003a). As labeled in the left panel, the dashed lines are two simulations drawn from the master ensemble: UCLA-0 (long dash) and UCLA-1 (short dash). Horizontal dashed lines delimit cloud area. The shading is as in Fig. 2 and as described in the text.

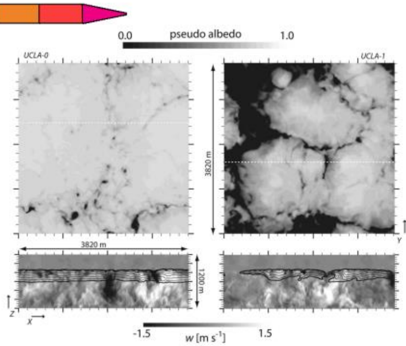

FIG. 8. (top) Visualization of flow fields from (left) UCLA-0 and (right) UCLA-1 simulations at the end of the simulation period. Shown are (top) plan-view images of the albedo estimated from the liquid water path, and (bottom) cross sections showing vertical velocity (shaded) and cloud water (contoured). The cross-section cuts are indicated by the white dashed line in plan-view plots. These fields are drawn from simulations wherein $N_x = N_y = 192$ and $\Delta x = \Delta y = 20$ m. The change in the horizontal mesh leads to more pleasing flow visualization, but has no marked impact on the flow statistics.

UCLA-LESの結果

雲水・簡易的な放射のみ導入→モデル間の相違は大幅増

対流混合層の比較実験まとめ

- ドライの対流混合層のLESによる再現はロバスト
  - コードのバグのチェックにも利用できる
- サブグリッドモデルにはあまり依存しない→グリッドスケールのダイナミクスでほぼ決定
- 高次の物理量ほど不確定性は大きい
  - 例えば、4次の項がどれくらい信用できるか不明

- 湿潤過程を導入すると、不確定性が格段に大きくなる←何が正解か不明？観測に合わせる？

LESに必要な解像度は？

The Effect of Mesh Resolution on Convective Boundary Layer Statistics and Structures Generated by Large-Eddy Simulation

PETER P. SULLIVAN AND EDWARD G. PAT

National Center for Atmospheric Research, Boulder, Col

(Manuscript received 17 November 2010, in final form 15 Feb

TABLE 1. Simulation grid spacings.

Run	Grid points	$(\Delta x, \Delta y, \Delta z)$ (m)	Δ_f (m)
A	32^3	(160, 160, 64)	154
B	64^3	(80, 80, 32)	77.2
C	128^3	(40, 40, 16)	38.6
D	256^3	(20, 20, 8)	19.3
E	512^3	(10, 10, 4)	9.6
F	1024^3	(5, 5, 2)	4.8

ABSTRACT

A massively parallel large-eddy simulation (LES) code for planetary boundary layers (PBLs) that utilizes pseudospectral differencing in horizontal planes and solves an elliptic pressure equation is described. As an application, this code is used to examine the numerical convergence of the three-dimensional time-dependent simulations of a weakly sheared daytime convective PBL on meshes varying from 32^3 to 1024^3 grid points. Based on the variation of the second-order statistics, energy spectra, and entrainment statistics, LES solutions converge provided there is adequate separation between the energy-containing eddies and those near the filter cutoff scale. For the convective PBL studied, the majority of the low-order moment statistics (means, variances, and fluxes) become grid independent when the ratio $z_i/(C_s\Delta_f) > 310$, where z_i is the boundary layer height, Δ_f is the filter cutoff scale, and C_s is the Smagorinsky constant. In this regime, the spectra show clear Kolmogorov inertial subrange scaling. The bulk entrainment rate determined from the time variation of the boundary layer height $w_e = dz_i/dt$ is a sensitive measure of the LES solution convergence; w_e becomes grid independent when the vertical grid resolution is able to capture both the mean structure of the overlying inversion and the turbulence. For all mesh resolutions used, the vertical temperature flux profile varies linearly over the interior of the boundary layer and the minimum temperature flux is approximately −0.2 of the surface heat flux. Thus, these metrics are inadequate measures of solution convergence. The variation of the vertical velocity skewness and third-order moments expose the LES's sensitivity to grid resolution.

おおよその見積もり

Sullivan and Patton(2011)の統計量に収束がみられる条件

- 条件はh/(CsＸdx)>310
- スマゴリンスキー定数Cs～0.2
- 混合層高さh=1kmならdx<16m、h=2kmならdx<32m

LESを利用した研究例

ニュース映像

Introduction

- An aircraft accident at 6/20/2012 1322JST
- Landing aircraft is seriously damaged

- Official accident analysis report conclude strong turbulence was caused by local topography

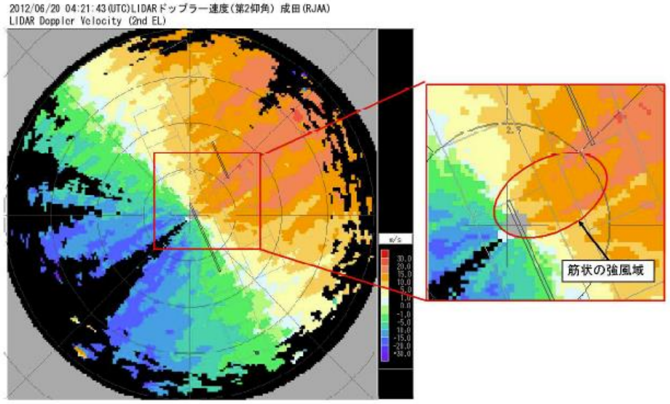

図2. 6. 3(1)　ドップラー速度観測データ（仰角2°）

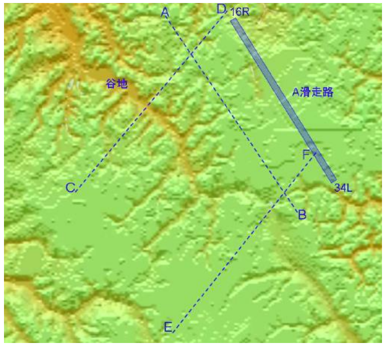

By official accident analysis

- Lidar observations and aircraft sensors→ Strong turbulence caused by convection rolls？ （Yoshino, submitted ）

Weather overview

Surface weather map (6/20/2012 09JST)

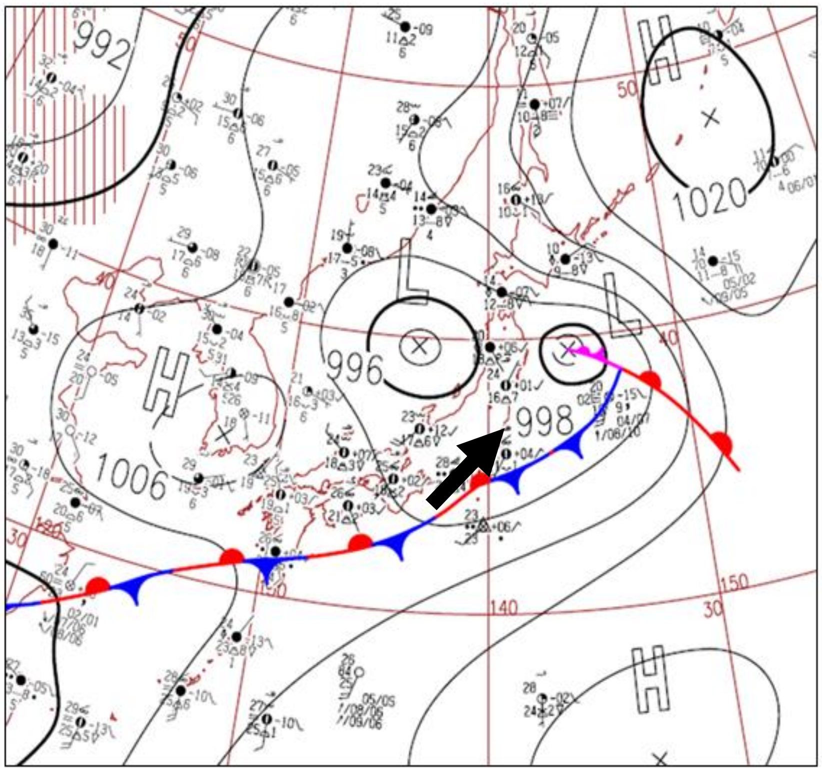

Weather observatory report near Narita Airport (Sakura) on 6/20/2012

佐倉　2012年6月20日（1時間ごとの値）

時	降水量 (mm)	気温 (℃)	風速・風向(m/s)		日照時間 (h)	雪(cm)	
			風速	風向		降雪	積雪
1	0.5	25.6	13.8	南南西		///	///
2	0.0	25.3	13.8	南西		///	///
3	0.0	24.6	10.0	南南西		///	///
4	0.0	24.3	9.4	南南西		///	///
5	0.0	24.4	10.3	南西	0.0	///	///
6	0.0	24.8	7.8	南南西	1.0	///	///
7	0.0	25.5	9.2	南南西	0.9	///	///
8	0.0	26.9	7.7	南西	1.0	///	///
9	0.0	28.1	8.0	南西	1.0	///	///
10	0.0	28.0	8.1	南西	0.9	///	///
11	0.0	27.8	9.0	南西	0.7	///	///
12	0.0	27.8	8.4	南西	0.6	///	///
13	0.0	28.0	8.0	南西	0.3	///	///
14	0.0	27.6	8.6	南西	0.1	///	///
15	0.0	28.0	9.1	南西	0.1	///	///
16	0.0	27.1	10.9	南西	0.0	///	///
17	0.0	26.3	8.3	南西	0.0	///	///
18	0.0	26.0	7.0	南西	0.0	///	///
19	0.0	25.5	7.1	南西	0.0	///	///
20	0.0	25.6	4.9	南南西		///	///
21	0.0	24.2	1.0	北		///	///
22	0.0	21.2	2.2	北北東		///	///
23	0.0	19.7	3.2	北北東		///	///
24	0.0	19.5	2.3	北北東		///	///

Fine (Morning) and partial cloudy (Afternoon), Strong south-westerly

Purpose

- Perform numerical weather prediction on the case of the accident (6/20/2012)
- Large eddy simulation (LES) to explicitly resolve near-surface turbulence structures

↓

- Investigate characteristics of **low level jet in the environment** and **turbulence near the surface**
- Validated by Lidar and aircraft observations
- Confirm strong turbulence is caused by **convection rolls**

Model setup

- JMA's non-hydrostatic model (Saito et al., 2006)
- Outer run
  - Horizontal resolution dx: 1km
  - Grid numbers: 800 × 800 × 80
  - Turbulence parameterization: Deardroff
  - Initial & boundary conditions: MANL by JMA
  - Initial time: 0900JST
- Inner (LES) run
  - Horizontal resolution dx: 100m
  - Grid numbers: 1200 × 1200 × 80
  - Turbulence: Deardroff
  - Initial & boundary conditions: every 30 mins. outputs from outer run
  - Initial time: 1200JST

Surface wind speed (z^*=10m) in whole computational domain

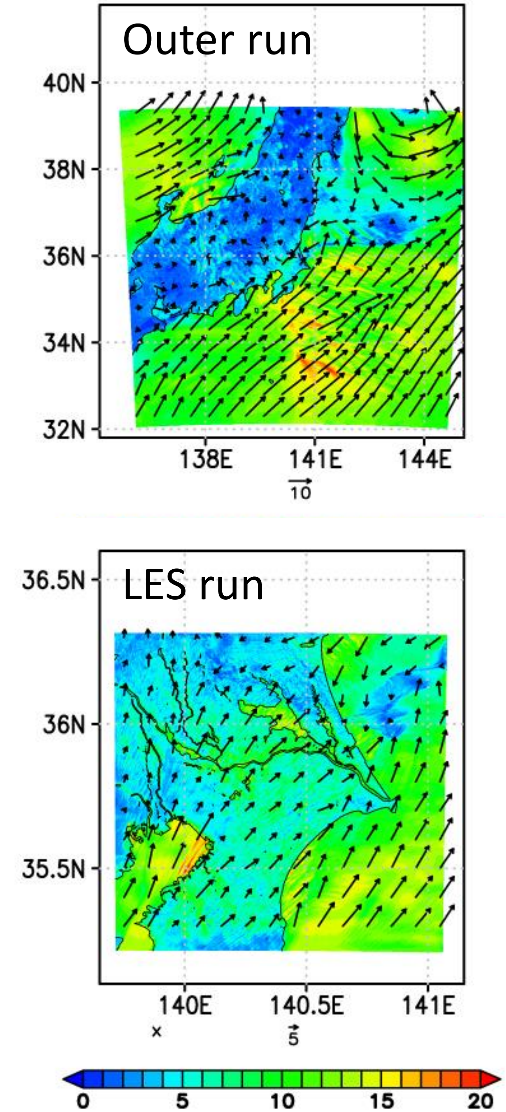

Deardroffモデル

$$\frac{\partial \bar{E}}{\partial t} = -\frac{\partial}{\partial x_i}(\bar{u}_i \bar{E}) - \overline{u'_i u'_j}\frac{\partial \bar{u}_i}{\partial x_j} + \frac{g}{\theta_0}\overline{w'\theta'_v} - \frac{\partial}{\partial x_i}[\overline{u'_i(e' + p'/\rho_0)}] - \varepsilon$$

where $e' \equiv \frac{1}{2}(u'^2 + v'^2 + w'^2)$ and ε is the rate of dissipation within the grid
The subgrid fluxes were parameterized by

$$\overline{u'_i u'_j} = -K_m(\partial \bar{u}_i/\partial x_j + \partial \bar{u}_j/\partial x_i) + (2/3)\delta_{ij}\bar{E}$$

$$\overline{u'_i \theta'_l} = -K_h \partial \bar{\theta}_l/\partial x_i$$

Localなモデル

Outer run: low level south-westerly jet

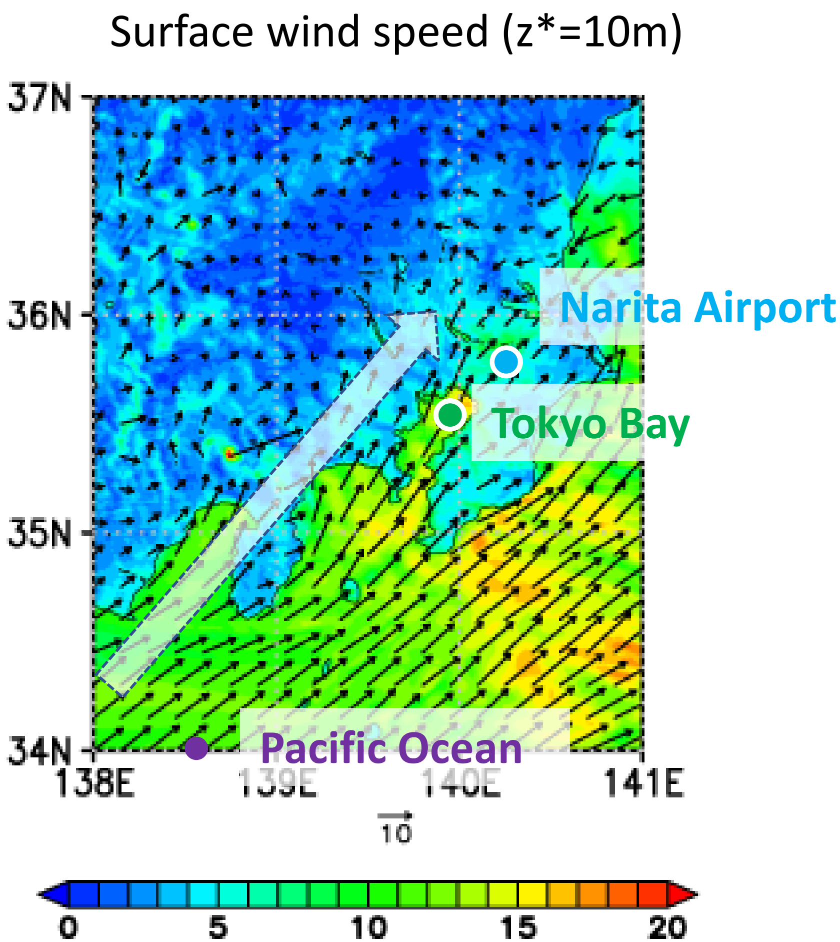

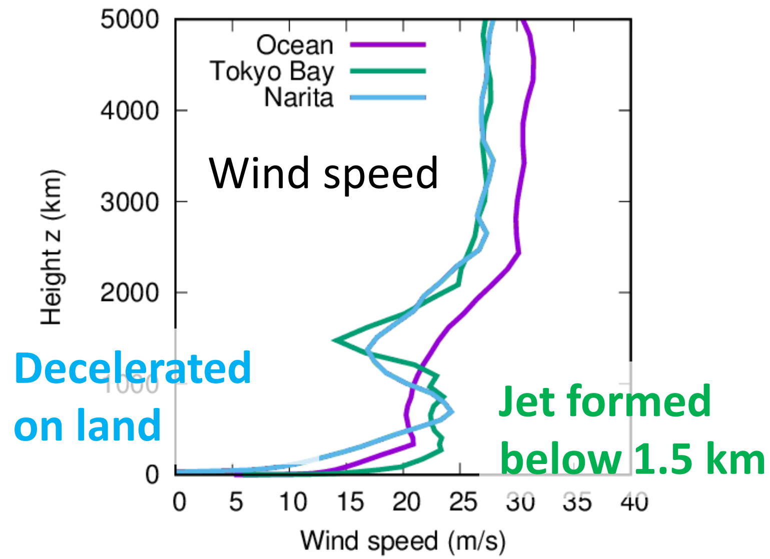

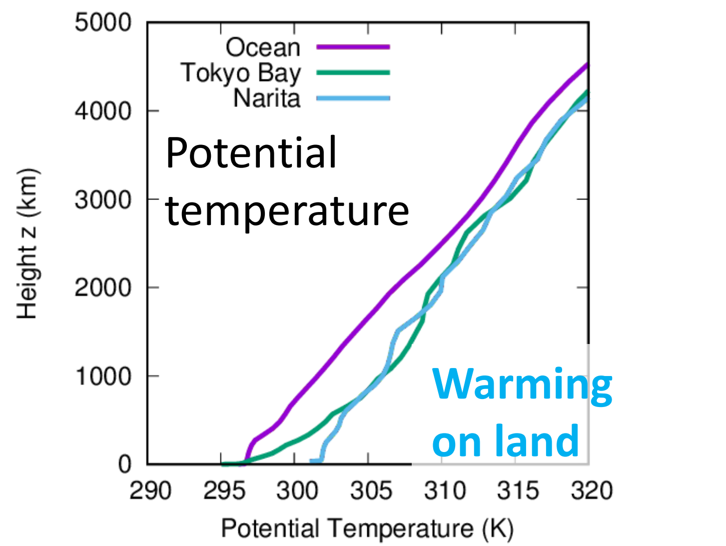

Winds and potential temperature in east-west vertical cross-section

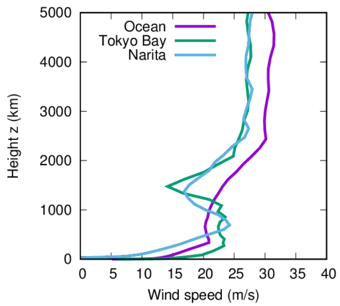

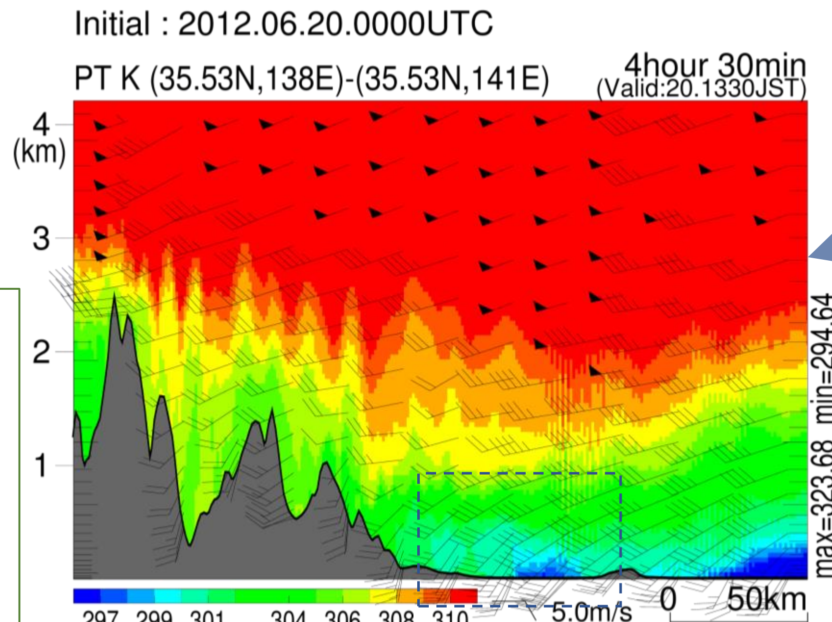

Tokyo Bay

Surface wind (z*=10m)

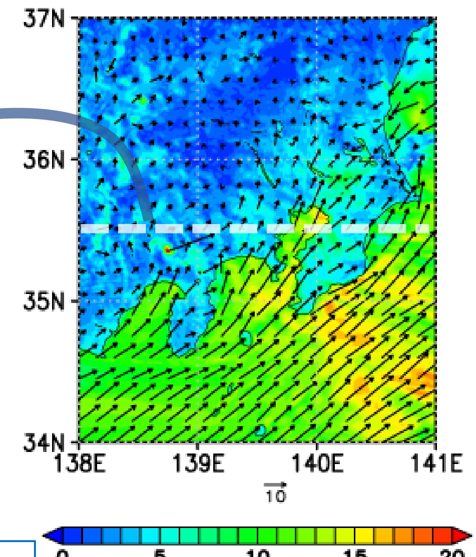

Weaker and Warmer westerly from central mountain range

Colder South-westerly from pacific ocean

A sensitivity experiment without topography

Entire computation domain and surface wind (z*=10m)

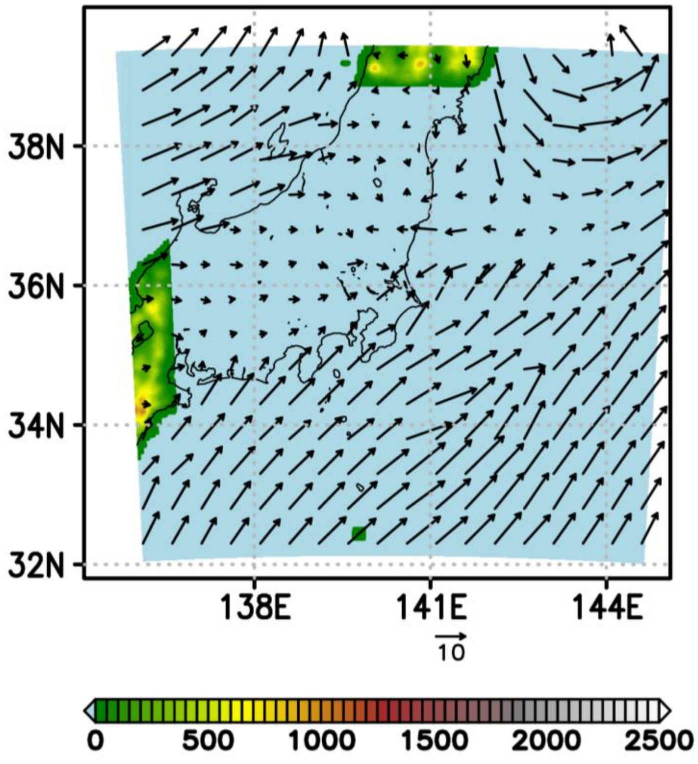

Wind speed difference (z*=5m): [No topography] – [Control]

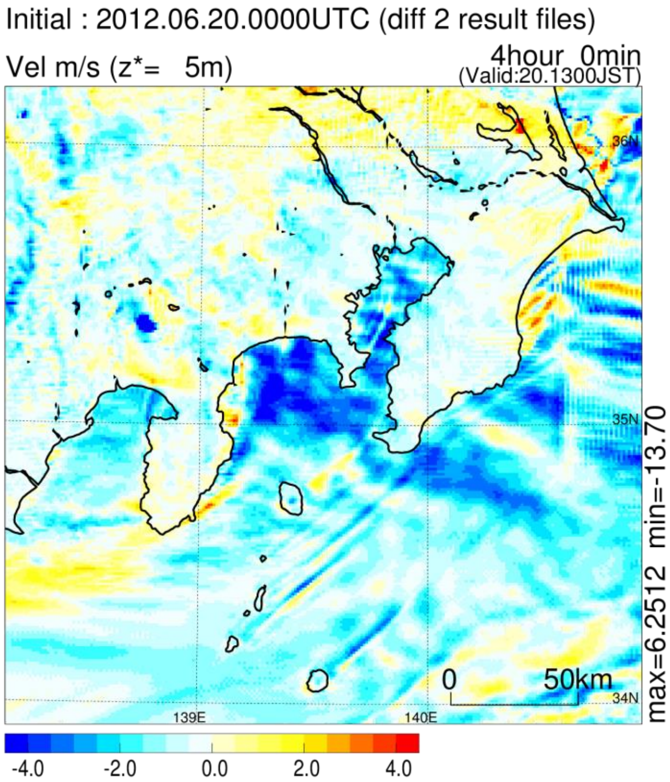

→ Blocking of central mountain ranges accelerate low-level winds on Tokyo bay in outer run

Inner (LES) run

Vertical profiles around Narita Airport@ 1330JST

Horizontal wind speeds

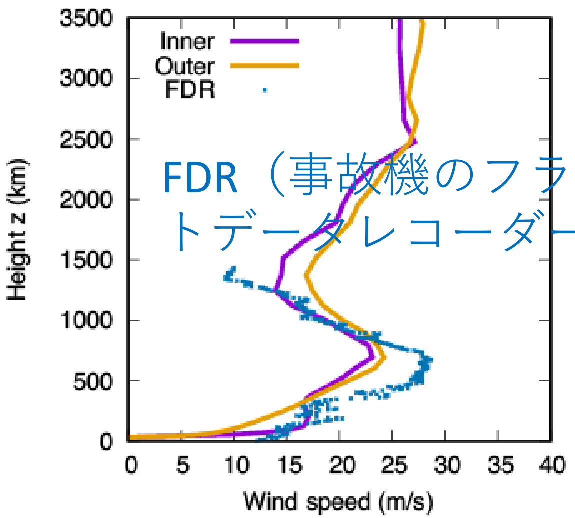

Wind direction

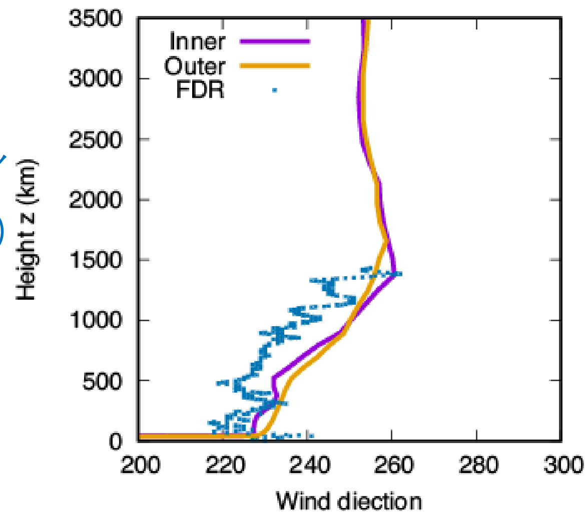

Potential temperature

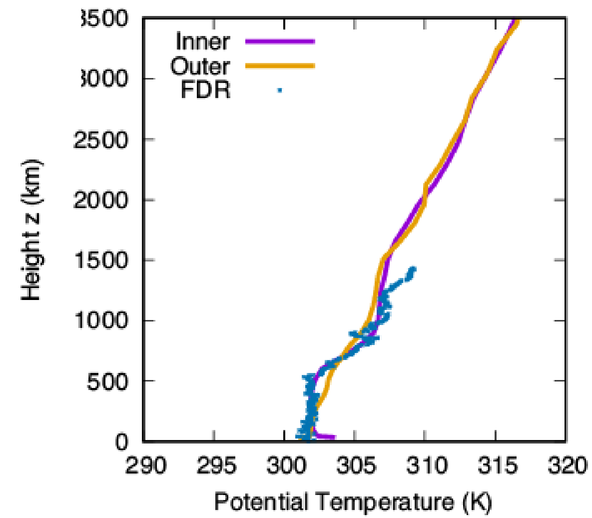

→ Strong vertical shear in boundary layer

→ Typical vertical profile of convective mixed layer only in Inner run

- Roll convection (z/L~0, e.g., Asai 1970) is expected
- **Inner-run result is more reasonable**

Horizontal wind speed (z*=15 m) around Narita Airport

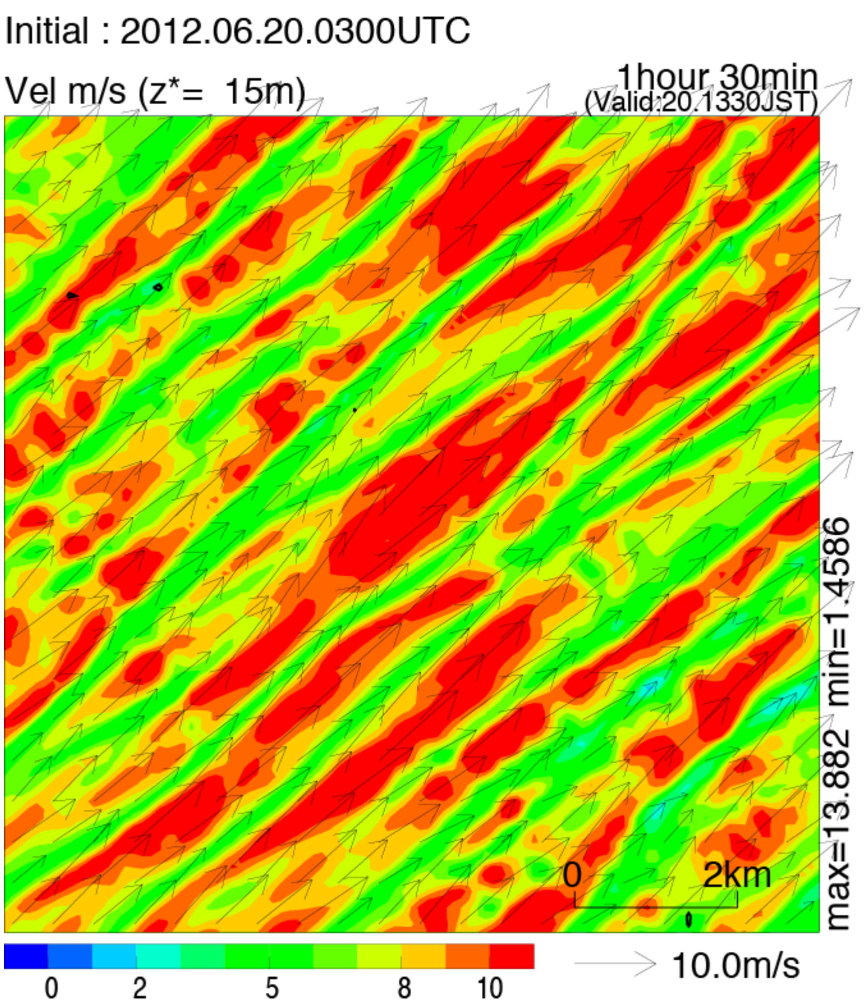

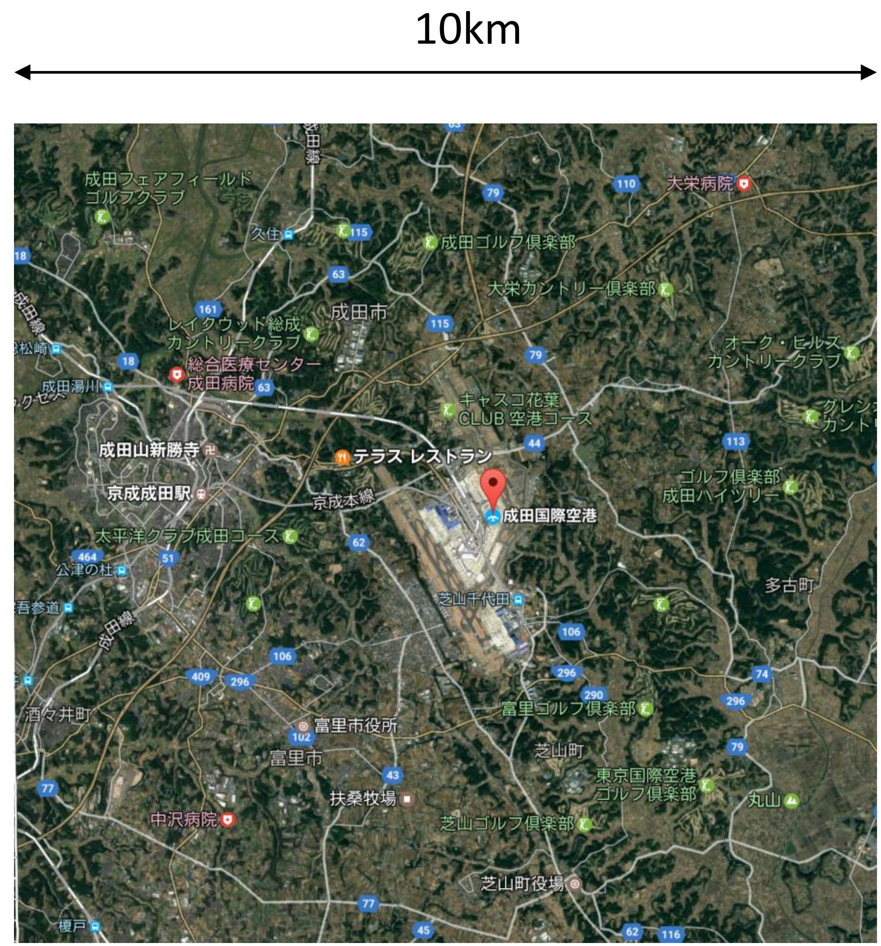

Compared with Doppler velocity of Lidar obs. (Yoshino, submitted)

Angle of elevation 2°

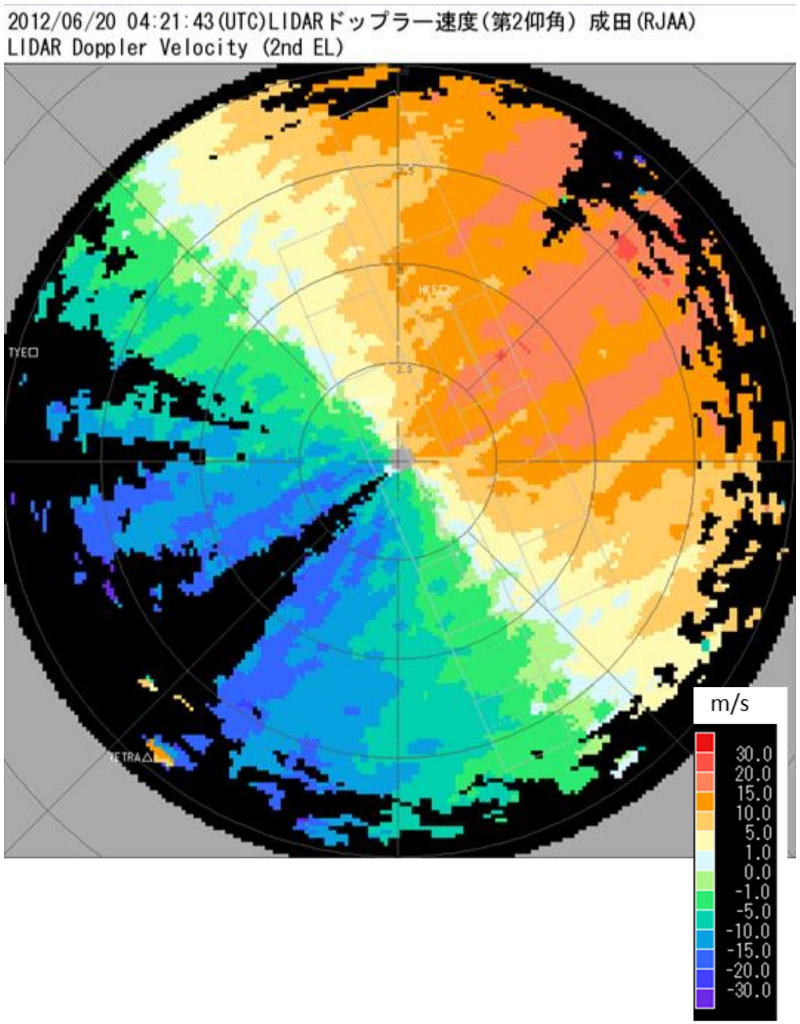

LES run

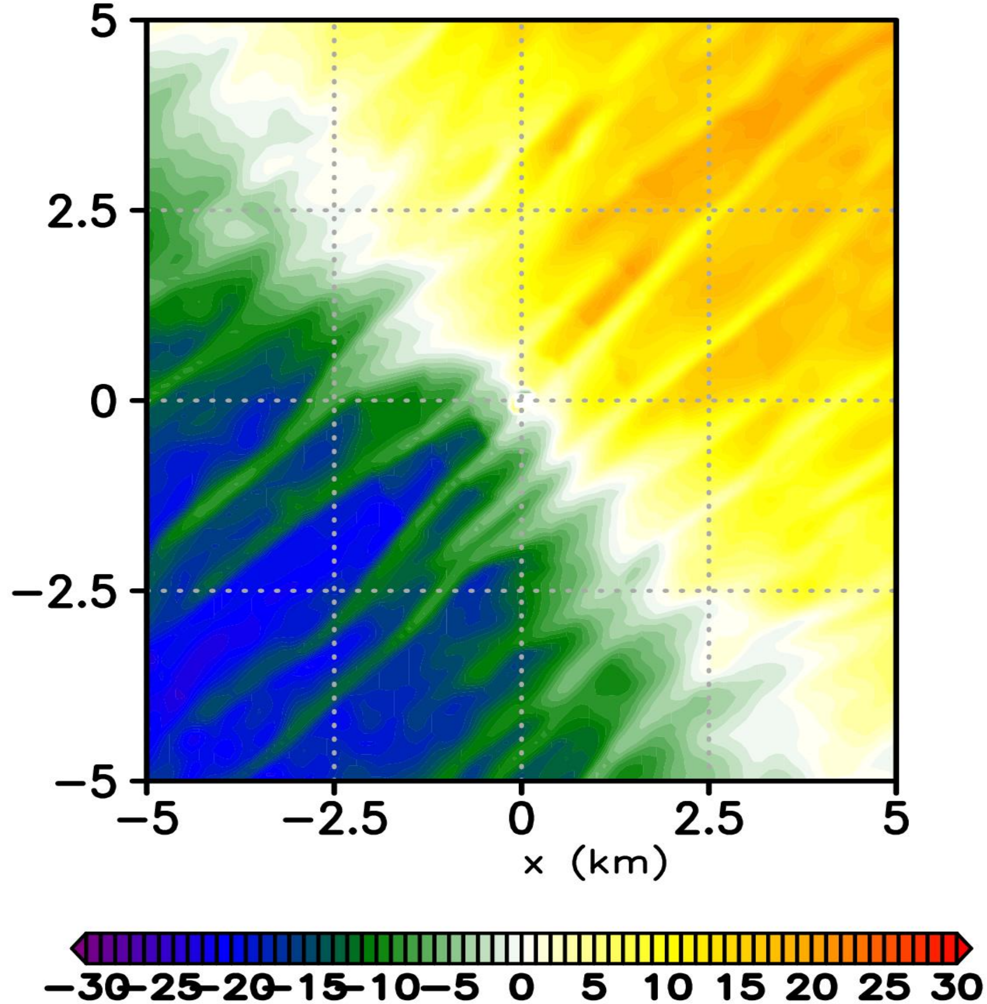

Horizontal velocity along runway of Narita Airport

z=165 m

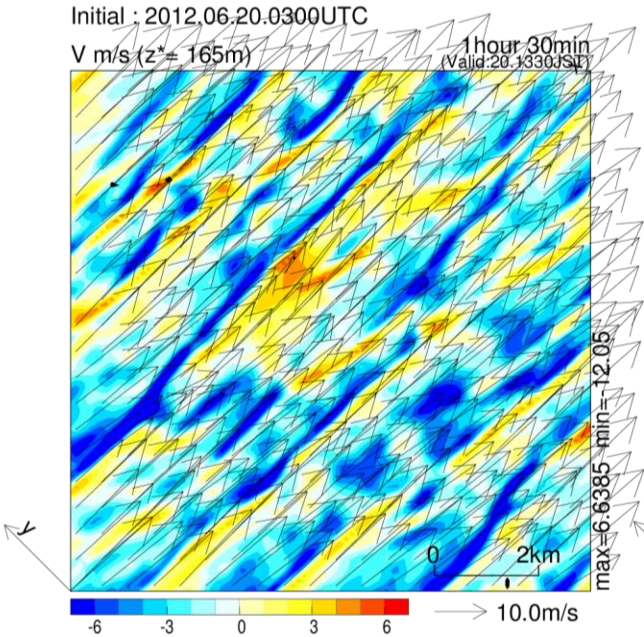

z=15 m

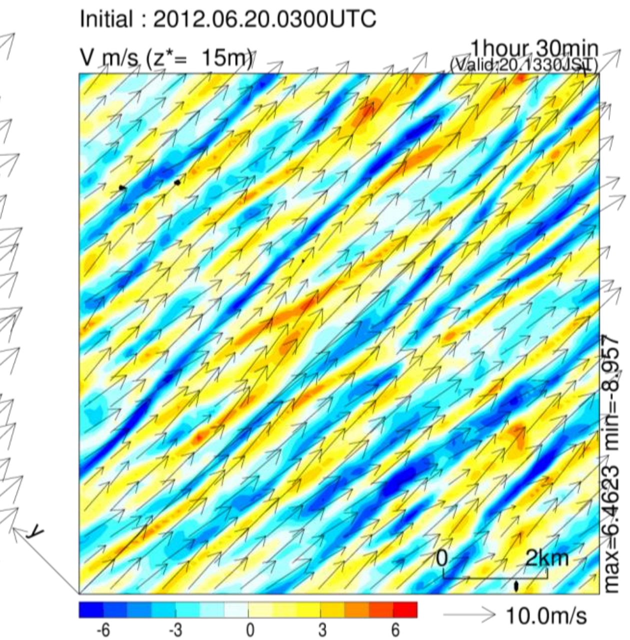

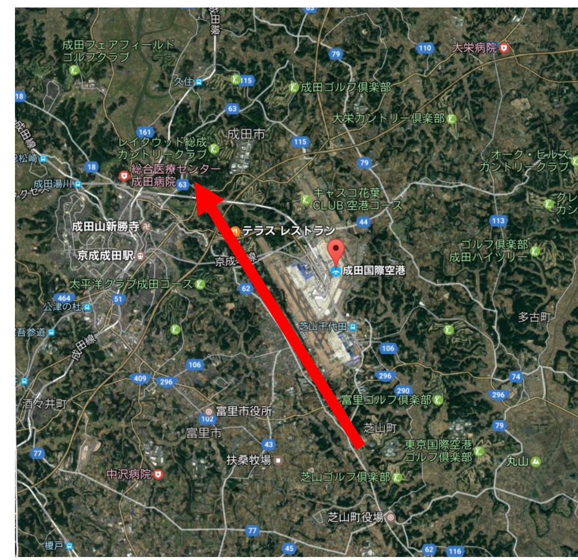

~ 10m/s difference between 500m along landing path

Convection rolls on land

Vertical velocity at z*=304 m

50km

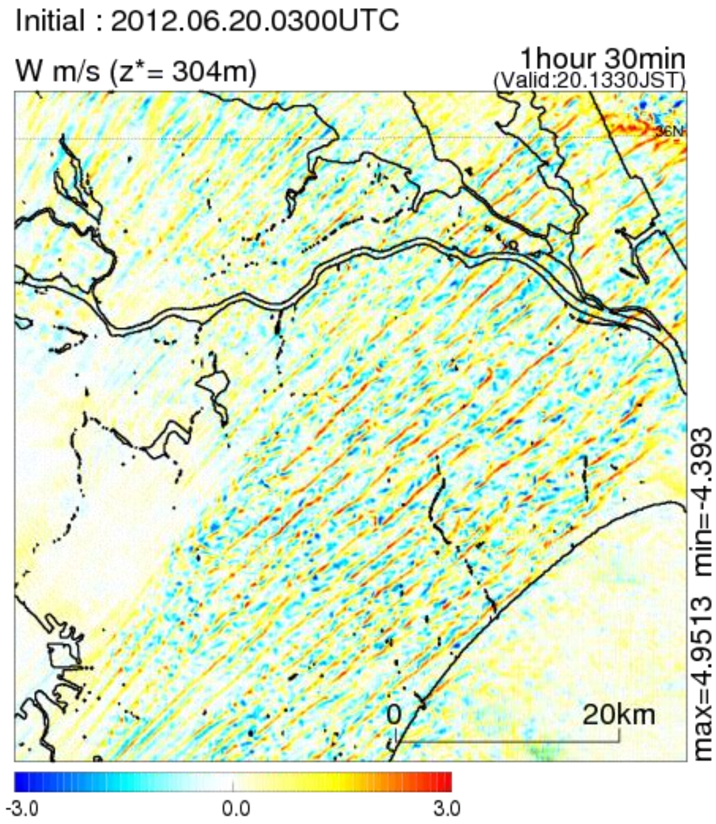

Convection rolls are widespread over land
→ Rolls were not due to local topography

Observation: Doppler spectrum width (Yoshino, submitted)

Hypothesis:

Larger Doppler spectrum width → Larger TKE → Updraft?

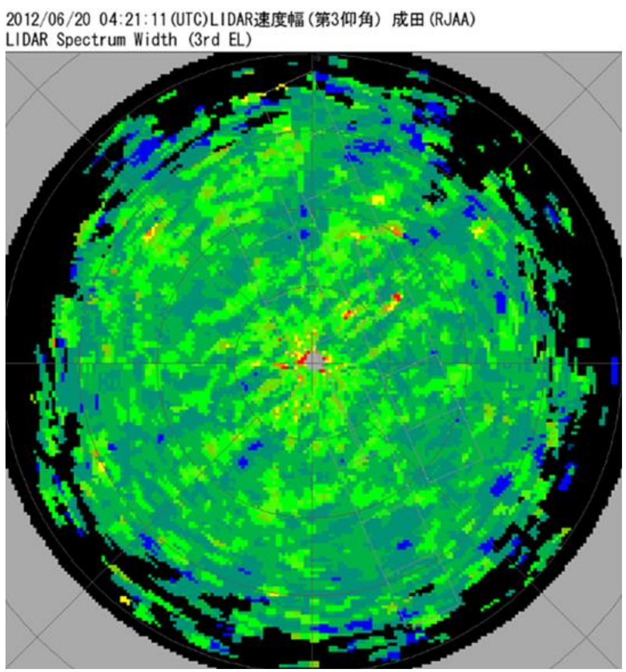

TKE in simulation

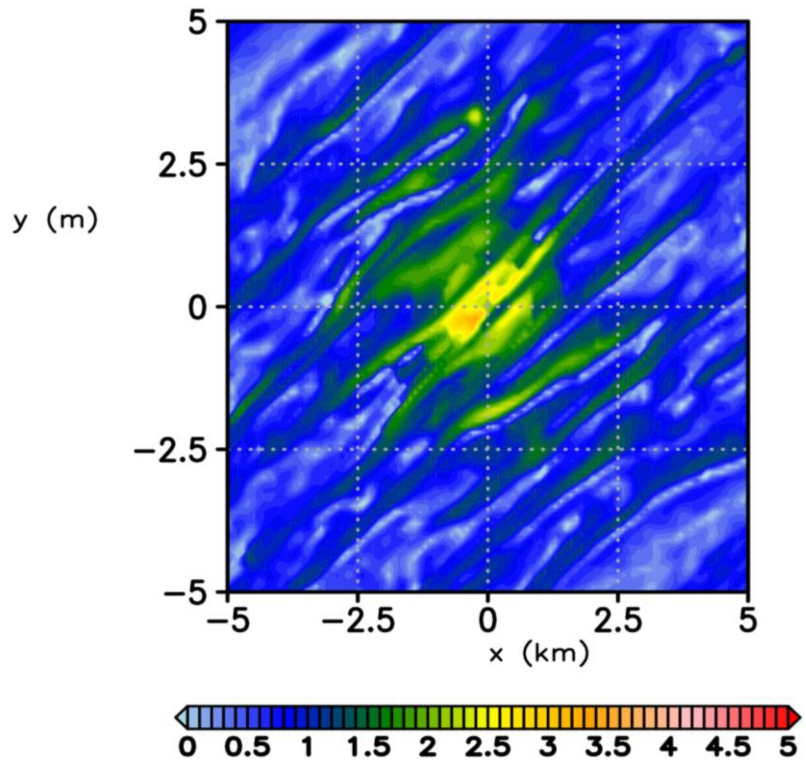

TKE and vertical velocity *w* in vertical plane

TKE (shade) & w (contours)

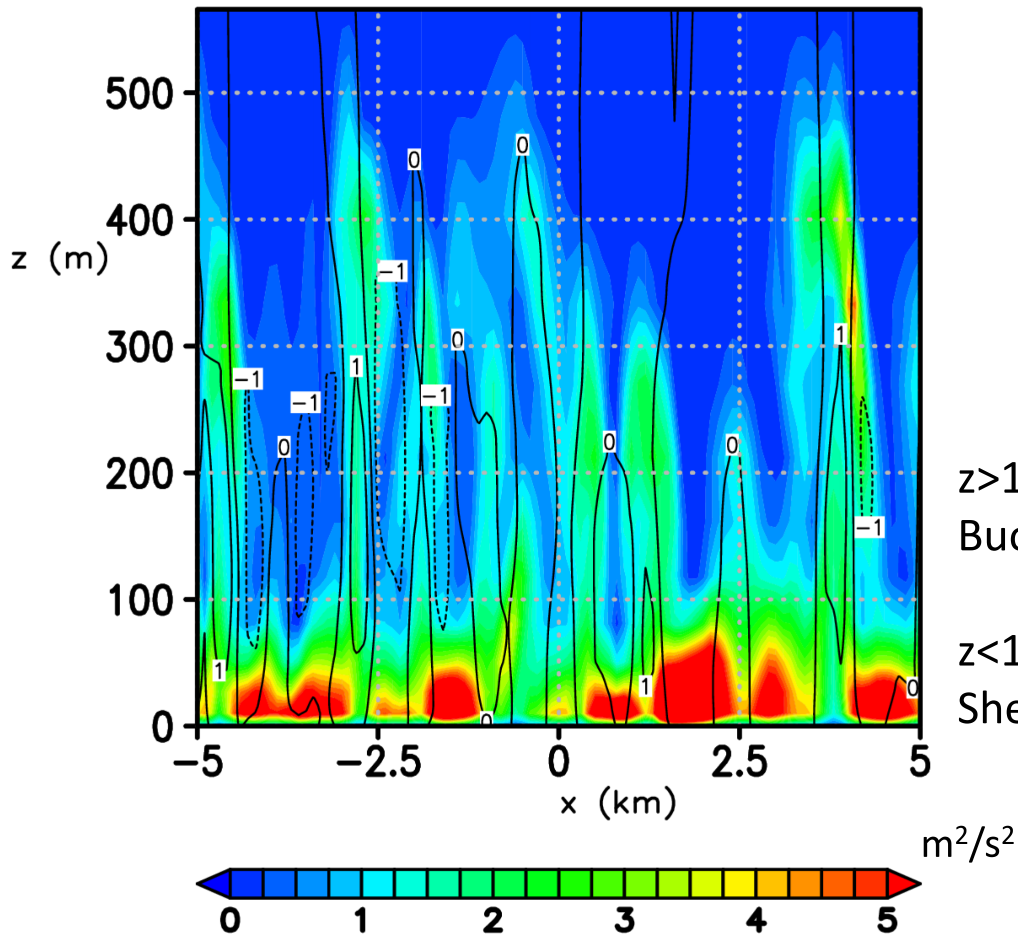

z>100m: Larger TKE in updraft (w>0)
Buoyancy production

z<100m: Larger TKE in downdraft (w<0)
Shear production

Summary

Numerical weather prediction model is used to reproduce the strong turbulence at Narita Airport in the case of an aircraft accident

Successfully reproduced

- Environmental wind in outer run (dx=1km)
- Turbulence structures in LES run (dx=100m)

Mechanism

- Incoming south-westerly is accelerated on Tokyo bay due to blocking of central mountain range
- Roll convection occur under strong vertical shear over the heated land

LES is useful for assessment and forecast of local phenomena